5. SITE 983[1]

Shipboard Scientific Party[2]

HOLE 983A

Position: 60°24.200′N, 23°38.437′W

Start hole: 1200 hr, 21 July 1995

End hole: 0930 hr, 22 July 1995

Time on hole: 21.5 hr (0.90 days)

Seafloor (drill pipe measurement from rig floor, mbrf): 1994.1

Total depth (drill pipe measurement from rig floor, mbrf): 2248.5

Distance between rig floor and sea level (m): 11.1

Water depth (drill pipe measurement from sea level, m): 1983.0

Penetration (mbsf): 254.4

Coring totals:
Type: APC
Number: 27
Cored: 254.4 m
Recovered: 264.42 m, 103.9%

Formation:
Unit I: 0–254.4 mbsf; Holocene to late Pliocene; clay with silt, nannofossils, mixed sediment

HOLE 983B

Position: 60°24.210′N, 23°38.437′W

Start hole: 0930 hr, 22 July 1995

End hole: 0315 hr, 23 July 1995

Time on hole: 17.75 hr (0.74 days)

Seafloor (drill pipe measurement from rig floor, mbrf): 1993.8

Total depth (drill pipe measurement from rig floor, mbrf): 2245.5

Distance between rig floor and sea level (m): 11.1

Water depth (drill pipe measurement from sea level, m): 1982.7

Penetration (mbsf): 251.7

Coring totals:
Type: APC
Number: 27
Cored: 251.7 m
Recovered: 261.83 m, 104.0%

Formation:
Unit I: 0–251.7 mbsf; Holocene to late Pliocene; clay with silt, nannofossils, mixed sediment

[1]Jansen, E., Raymo, M.E., Blum, P., et al., 1996. *Proc. ODP, Init. Repts.,* 162: College Station, TX (Ocean Drilling Program).
[2]Shipboard Scientific Party is given in the list preceding the Table of Contents.

HOLE 983C

Position: 60°24.218′N, 23°38.443′W

Start hole: 0315 hr, 23 July 1995

End hole: 0200 hr, 24 July 1995

Time on hole: 22.75 hr (0.95 days)

Seafloor (drill pipe measurement from rig floor, mbrf): 1996.1

Total depth (drill pipe measurement from rig floor, mbrf): 2256.5

Distance between rig floor and sea level (m): 11.1

Water depth (drill pipe measurement from sea level, m): 1985.0

Penetration (meters below seafloor, mbsf): 260.4

Coring totals:
Type: APC
Number: 28
Cored: 260.4 m
Recovered: 271.75 m, 104.4%

Formation:
Unit I: 0–260.4 mbsf; Holocene to late Pliocene; clay with silt, nannofossils, mixed sediment

Principal results: Site 983 is located on the Bjorn Drift in approximately 1650 m water depth on the eastern flank of the Reykjanes Ridge. A sequence of sediments ranging in age from late Pliocene to Holocene (2.0 to 0 Ma) was recovered at Site 983. Age estimates are consistent between biostratigraphic and magnetic data and indicate that the Site 983 sedimentary sequence is continuous, without significant hiatuses. Sedimentation rates were determined using magnetic polarity data combined with the biostratigraphic datums and range from 9 cm/k.y. in the Pleistocene, up to 17 cm/k.y. in the upper Pliocene section. Multisensor track (MST) data allowed the construction of a continuous composite section for this site and preliminary studies done on board indicate strong variance in a number of parameters on both Milankovitch and sub-Milankovitch time scales, throughout the section.

The sediments at Site 983 are predominantly composed of rapidly accumulated fine-grained terrigenous particles with minor amounts of biocarbonate and biosilica. Although discrete ash layers are rare, pale to dark brown glass (tachylyte) commonly occurs as a constituent of the silt and sand size fractions. Authigenic iron sulfides, primarily in the form of disseminated pyrite, are also typically present. The dominant lithologies include silty clay, clay, clayey nannofossil mixed sediment, and clay with variable amounts of nannofossils and silt. Nannofossil oozes with variable amounts of clay and sponge spicules also occur. Lithologic variation on decimeter to meter scales characterizes the sediment at this site and is due to changes in the abundance of silt and biogenic materials relative to clay content. The range of variation in these components is diminished relative to sediments of comparable age at Sites 980 to 982.

No major lithologic boundaries occur within the 260 m of sediment recovered at this site and one lithologic unit is recognized. Subtle, but distinct, boundaries that demark three subunits occur at depths of 120 mbsf and 180 mbsf. The shallower boundary is recognized primarily in the spectral reflectance signal. It is characterized by a downcore decrease in the amplitude of the higher frequency (decimeter- to meter-scale) reflec-

tance signal and an absence of the lower frequency reflectance signal (>10-m scale). The deeper boundary is recognized in visual examination of split cores and smear slides. It is characterized by a downcore absence of layers in which biocarbonate is predominant. All dropstones, which are never common, occur above this deeper horizon. There is no evidence of significant sediment disturbance, winnowing, or erosion at Site 983 although bioturbation is ubiquitous throughout the cores.

Calcium carbonate contents fluctuate between 0.7% and 43.3% with an average value of 16.8%, gradually decreasing with increasing sediment depth. As at Sites 980, 981, and 982, the carbonate cycles of Hole 983A probably reflect glacial/interglacial fluctuations. Total organic carbon (TOC) contents vary between 0.04% and 0.48%, with an average value of 0.18%. Total nitrogen and sulfur contents are generally very low. C/N ratios between 1 and 10 are indicative of predominantly marine organic material.

Calcareous nannofossils are the dominant fossil group at this site and are generally abundant and well preserved. All the standard Quaternary nannofossil zones are recognizable. Planktonic foraminifers are generally common to abundant and well preserved throughout the uppermost Pliocene to Holocene sequence although rare barren intervals are observed. Benthic foraminifers are present at most of the levels examined and preservation is good throughout. Diatoms at Site 983 were common to abundant and exhibit moderate to good preservation. Due to the possible influence of the East Greenland Current, warmer water species were rare while many cooler water indicators were more common. Siliceous flagellates (including silicoflagellates, ebridians, and actiniscidians) range from trace to common in abundance with good to moderate preservation.

All archive halves of Holes 983A, 983B, and 983C were measured using the pass-through cryogenic magnetometer. The Brunhes/Matuyama boundary and the Jaramillo and the Olduvai Subchrons are well defined in all three holes. A prominent normal-polarity subchron observed in the three holes between the Jaramillo and the Olduvai Subchrons is tentatively identified as the Cobb Mountain event. The high magnetic remanence intensities and high sedimentation rates of the sediments from this site will enable very interesting shore-based work on magnetic field transitions and possible secular field changes.

Pore-water profiles from Site 983 are typical of sediments in which sulfate reduction and methanogenesis are occurring. Sulfate concentrations decrease from seawater values at the top of the core to zero at about 100 mbsf. Below 120 mbsf, methane begins to increase from 0 ppm, reaching a maximum of about 9000 ppm near the base of the hole. The boundary between sulfate reduction and methanogenesis is very sharp at 120 mbsf, presumably because utilization of methane by sulfate-reducing bacteria prevents significant diffusive penetration of methane into the sulfate reduction zone above. The sharp sulfate/methane boundary at 120 mbsf also corresponds with lithologic subboundary IA/IB and with seismic reflector R2. Ethane and propane values occur in detectable amounts below 165 mbsf; however, the high C_1/C_2 ratios also suggest that the source for methane is most likely in situ bacterial methanogenesis resulting from decomposition of organic matter in the sediments.

Bulk density, velocity, and shear strength all gradually increase downcore. The physical properties suggest a stratigraphically continuous sequence and the drilled section has been defined as one geotechnical unit.

The seismic survey, on the other hand, resulted in the designation of seven seismic units, (GA-I to GA-VII), with the upper five being cored at Site 983. The sedimentary section as a whole is acoustically well-stratified, although with variation between units. Lateral changes in sediment thickness are common and seem to be controlled by basement relief as well as depositional and erosional processes. The seismic reflectors (R1 to R6), marking changes in seismic character, are also unconformities when traced laterally away from Site 983. At Site 983, all seismic reflectors appear conformable, further testifying to the completeness of the site.

BACKGROUND AND OBJECTIVES

Site 983 (GARDAR-1) is located on the Gardar Drift in approximately 1985 m water depth on the eastern flank of the Reykjanes Ridge (Fig. 1). The primary drilling objective at Site 983 was to recover high-sedimentation-rate pelagic sequences with which to study climate evolution in the North Atlantic region over the last few million years. The site is located near the approximate boundary of Gla-

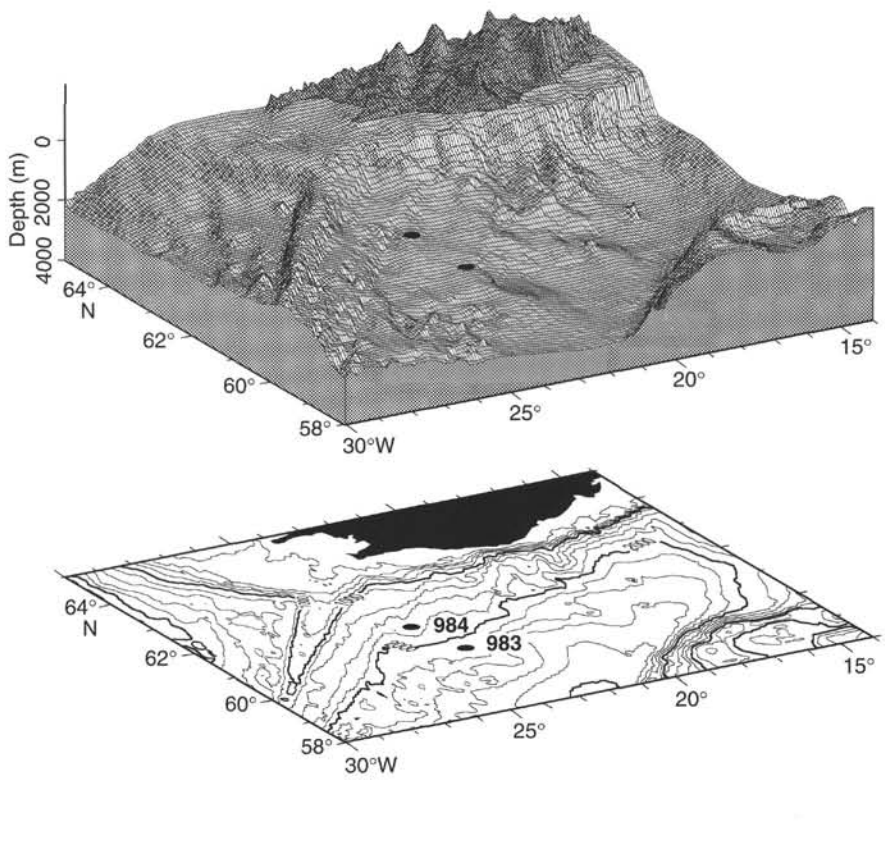

Figure 1. Detailed topographic view of Gardar and Bjorn Drift region showing location of Sites 983 and 984.

cial North Atlantic Intermediate Water (GNAIW) and Southern Source Water (SSW) during the last glaciation (Oppo and Lehman, 1993). Obtaining a long-term history of this GNAIW is one of the primary scientific objectives of this site. In conjunction with Sites 980, 981, and 982 to the east, and Site 984 just to the north, this site forms a depth transect of five sites roughly spanning the interval between 1 and 2 km water depth.

This same suite of sites also defines a northwest-southeast transect extending from ~24°W to ~14°W. Intercomparison of carbonate, faunal, and geochemical records from these sites should define changes in surface-water temperature and hydrography over the Pliocene-Pleistocene. In addition, Site 983 should prove very sensitive to Nordic Seas overflows across the Greenland-Scotland Ridge. This site lies on the northwest margin of the Iceland Basin directly downstream of overflows from the Iceland-Faeroe Ridge (see fig. 1, chapter 1, this volume). This water passes as a deep northern boundary current through the Charlie-Gibbs Fracture Zone south of Site 983 (e.g., McCartney, 1992). Using this site, along with the other sites drilled north and south of the Greenland-Scotland Ridge, we hope to unravel the long-term history of deep- and intermediate-water formation in the Nordic Seas and subpolar North Atlantic. Comparison of $\delta^{13}C$ and trace element gradients between these sites should allow us to define glacial-interglacial changes in North Atlantic Intermediate Water formation.

As predicted from previously studied piston and gravity cores in the region, we recovered a sedimentary sequence with unusually high sedimentation rates (between 10 and 20 cm/k.y.). This will provide us with an unprecedented record of both glacial-interglacial and millennial-scale variations in thermohaline circulation, surface-water temperatures, and ice-rafting history over the late Pliocene and Pleistocene. In particular, we plan to investigate rapid century- to millennial-scale oscillations, such as those observed in temperature and dustiness in Greenland ice cores (Dansgaard-Oeschger events), as well as in late Pleistocene marine record (e.g., Bond et al., 1992, 1993; Bond and Lotti, 1995; Fronval et al., 1995). In piston cores, such events can be seen as changes in surface foraminiferal fauna (sea-surface temperature), carbonate, color, and deep-ocean chemistry. The transitions between cold and warm epochs in ice cores are abrupt: ~6°C warmings occur in as little as 10–20 years and four-fold drops in dust content in as little as 20 years. Broecker (1994) reviews possible causes for these oscillations and the linkages between deep-sea sedimentation and ice-core records. One possibility is that millennial-scale climate variations in ice cores are related to the strength of the thermohaline "conveyor belt."

Site 983 will be used to address a number of questions relating to these "sub-Milankovitch" cycles. In particular, we expect to determine whether these rapid climate oscillations characterized the marine record during earlier, warmer climatic regimes, for instance, during the late Pliocene. We will look for variations in color, foraminiferal faunal composition, stable isotope composition, and lithic concentration. Many of the continuous records of physical properties collected on the ship (e.g., MST and spectral reflectance data) will be used for this purpose, and an early research priority will be to determine how these signals relate to lithologic and textural variations in the sediment (e.g., Robinson and McCave, 1994).

Superimposed on the "Dansgaard-Oeschger" events of the last glacial period are "Heinrich" layers, events with longer characteristic repeat times (~10,000 yr), which may be related to surges of the eastern Laurentian and other major ice sheets (Heinrich, 1988; Bond et al., 1993; MacAyeal, 1993; Broecker, 1994; Fronval et al., 1995). Site 983 is located just north of the zonal axis of the Heinrich layers documented in the last glacial cycle. Determining the geographic distribution of these Heinrich events, their long-term character, and the timing of their first occurrence is a main objective of our drilling on the Feni (Sites 980 and 981), Gardar (Site 983), and Bjorn (Site 984) Drifts. Are they restricted to the "100-k.y. world" of the Brunhes Chron, which was characterized by large marine-based continental ice sheets? Do they occur in intervals characterized by higher frequency variations in smaller ice sheets? Are marine-based ice sheets a prerequisite for climatic instability of this sort? Do Heinrich events always have a characteristic repeat time of 10,000 years?

By studying deep-water variability using carbon isotopes, Cd/Ca ratios, and other proxies, we will also be able to determine whether millennial-scale variations in surface temperature are associated with variations in thermohaline circulation (Boyle and Keigwin, 1987; Rahmstorf, 1994; Weaver and Hughes, 1994; Oppo and Lehman, 1995). Combining data from Site 983 with that from shallower and deeper drift sites (Sites 980, 981, and 984), we will examine if, and how, changes in the vertical nutrient distribution in the North Atlantic occur. By studying sedimentation patterns, surface-water properties, and deep-water variability on suborbital time scales and relating these observations to ice cores, we hope to better understand the forcing and dynamics of decadal to millennial climate variability in the North Atlantic–Arctic region. The long-term perspective available from ODP drilling will significantly add to the knowledge from Greenland ice cores, which cover only the last 200 k.y.

OPERATIONS

Site 983 (GARDAR-1) was a high-priority contingency site which was drilled because the leg was ahead of schedule by nearly 2 days. The operational plan called for three piston-cored holes to approximately 300 m below seafloor. Because time was short, we decided to drill three shallower holes (<260 m) rather than two deeper holes.

Head winds limited the vessel's speed while en route to Site 983. Before slowing down for pre-site seismic profiling, the vessel averaged a mere 8.3 kt. At 0742 hr on 21 July 1995 the ship slowed down to 6.0 kt and the seismic gear was deployed for a limited pre-site survey of the site (see "Seismic Stratigraphy" section, this chapter). By 1158 hr on 21 July the seismic profiling gear had been recovered, the vessel had returned to the drilling location based on GPS coordinates, and the positioning beacon had been deployed, initiating Hole 983A.

A standard APC/XCB bottom-hole assembly was used for all holes at Site 983, including a nonmagnetic drill collar. Subsequent (B and C) holes were offset 15 m to the north. The mudline was established for each hole. The APC firing depth was offset by a few meters for subsequent holes to establish continuous sediment sections. Position, depths, and coring totals for each hole are summarized at the top of this chapter. All cores are listed in Table 1.

Coring proceeded without incident at all three holes until scientific target depth had been reached. The following cores were oriented with the Tensor tool: 983A-3H through 27H; 983B-3H through 27H; and 983C-3H though 27H. The drill pipe was tripped above mudline, clearing the seafloor, and the positioning beacon was released and subsequently recovered at 2225 hr on 23 July. The vessel was secured for transit and got underway at 0200 hr 24 July 1995.

COMPOSITE DEPTHS

Based on correlations between magnetic susceptibility, natural gamma radiation, gamma-ray attenuation porosity (GRAPE), and spectral reflectance data, continuity of the sedimentary sequence was documented for the entire sequence drilled at Site 983, extending from the late Pliocene through the Holocene. A composite section was developed as discussed in the "Composite Depths" section, "Explanatory Notes" chapter (this volume). The depth offsets that comprise the composite depth section for Site 983 are given in Table 2. Continuity of the stratigraphic section was confirmed from the mudline to approximately 288 mcd (260 mbsf in Hole 983C).

MST records that were useful in correlation are displayed on the composite depth scale in Figure 2 (see also back pocket). High-amplitude magnetic susceptibility and GRAPE variations were used to determine depth offsets for the composite depth section. *P*-wave velocity and natural gamma radiation measurements were also collected over nearly the entire cored sequence of all holes at both sites. These measurements, combined with percentage spectral reflectance measurements (see "Lithostratigraphy" section, this chapter), were useful in constraining the hole-to-hole correlations.

Overlap between adjacent holes was documented throughout the composite depth section. Although the relative agreement of sedimentary features in adjacent holes was excellent, stretching and compression within the cored sequence occurred over most intervals. Because much of this distortion occurs on a scale of less than 9 m, it was not possible to align every sedimentary feature using only composite depth scale adjustments. Within-core, decimeter to centimeter depth scale adjustments would be required to align all sedimentary features simultaneously.

The expansion of the composite depth section relative to the mbsf depth scale results from physical expansion of the cores after recovery as well as stretching of the sequence during the coring process. This expansion is illustrated in Figure 3. Growth of the mcd scale relative to the mbsf scale is about 10% in all holes from Site 983.

Following construction of the composite depth section for Site 983, a single spliced record was assembled from the aligned cores as discussed in the "Explanatory Notes" chapter (this volume). The tie points for the Site 983 splice are given in Table 3. Spliced magnetic susceptibility, natural gamma radiation, and GRAPE density are shown in Figure 4.

LITHOSTRATIGRAPHY

The sediments at Site 983 are predominantly composed of rapidly accumulated fine-grained terrigenous particles, and have an average calcium carbonate content of approximately 16%. Biocarbonate and, to a lesser extent, biosilica are present in variable minor amounts. Whereas discrete ash layers are rare, pale to dark brown glass (tachylyte) commonly occurs as a constituent of the silt- and sand-sized fractions. Authigenic iron sulfides, primarily in the form of disseminated pyrite, are also typically present in minor abundances. The dominant lithologies include silty clay, clay, clayey nannofossil mixed sediment, and clay with variable amounts of nannofossils and silt. Nannofossil oozes with variable amounts of clay and sponge spicules also occur. Lithologic variation on decimeter to meter scales characterizes the sediment at this site, and is due to changes in the abundance of silt and biogenic materials relative to clay content. The range of variation in these components is diminished relative to sediments of comparable age at Sites 980, 981, and 982.

The primary lithostratigraphic unit and subunits for the Site 983 sedimentary sequence are defined on the basis of data obtained from seven sources: (1) visual observation of color, (2) smear slide examination, (3) bulk calcium carbonate measurements, (4) spectral reflectance measurements, (5) magnetic susceptibility measurements,

Table 1. Coring summary for Site 983.

Core	Date (July 1995)	Time (UTC)	Depth (mbsf)	Length cored (m)	Length recovered (m)	Recovery (%)
162-983A-						
1H	21	1635	0.0–7.4	7.4	7.42	100.0
2H	21	1700	7.4–16.9	9.5	9.91	104.0
3H	21	1740	16.9–26.4	9.5	9.99	105.0
4H	21	1815	26.4–35.9	9.5	9.97	105.0
5H	21	1845	35.9–45.4	9.5	10.07	106.0
6H	21	1920	45.4–54.9	9.5	9.98	105.0
7H	21	1950	54.9–64.4	9.5	9.95	105.0
8H	21	2020	64.4–73.9	9.5	9.93	104.0
9H	21	2055	73.9–83.4	9.5	9.96	105.0
10H	21	2130	83.4–92.9	9.5	9.92	104.0
11H	21	2210	92.9–102.4	9.5	9.91	104.0
12H	21	2240	102.4–111.9	9.5	9.98	105.0
13H	21	2310	111.9–121.4	9.5	9.92	104.0
14H	21	2345	121.4–130.9	9.5	9.95	105.0
15H	22	0025	130.9–140.4	9.5	10.06	105.9
16H	22	0105	140.4–149.9	9.5	9.87	104.0
17H	22	0145	149.9–159.4	9.5	9.81	103.0
18H	22	0220	159.4–168.9	9.5	9.91	104.0
19H	22	0310	168.9–178.4	9.5	9.95	105.0
20H	22	0345	178.4–187.9	9.5	9.90	104.0
21H	22	0420	187.9–197.4	9.5	9.85	103.0
22H	22	0455	197.4–206.9	9.5	9.68	102.0
23H	22	0535	206.9–216.4	9.5	9.80	103.0
24H	22	0615	216.4–225.9	9.5	9.63	101.0
25H	22	0650	225.9–235.4	9.5	9.57	101.0
26H	22	0730	235.4–244.9	9.5	9.62	101.0
27H	22	0810	244.9–254.4	9.5	9.91	104.0
			Coring totals:	254.4	264.4	103.9
162-983B-						
1H	22	1040	0.0–4.7	4.7	4.73	100.0
2H	22	1110	4.7–14.2	9.5	9.97	105.0
3H	22	1150	14.2–23.7	9.5	10.03	105.6
4H	22	1220	23.7–33.2	9.5	9.84	103.0
5H	22	1255	33.2–42.7	9.5	9.89	104.0
6H	22	1325	42.7–52.2	9.5	9.80	103.0
7H	22	1355	52.2–61.7	9.5	9.94	104.0
8H	22	1425	61.7–71.2	9.5	9.99	105.0
9H	22	1500	71.2–80.7	9.5	10.08	106.1
10H	22	1535	80.7–90.2	9.5	9.82	103.0
11H	22	1605	90.2–99.7	9.0	10.02	105.0
12H	22	1640	99.7–109.2	9.5	9.85	103.0
13H	22	1715	109.2–118.7	9.5	9.80	103.0
14H	22	1750	118.7–128.2	9.5	9.93	104.0
15H	22	1820	128.2–137.7	9.5	10.02	105.5
16H	22	1920	137.7–147.2	9.5	9.83	103.0
17H	22	1955	147.2–156.7	9.5	9.94	104.0
18H	22	2030	156.7–166.2	9.5	9.61	101.0
19H	22	2105	166.2–175.7	9.5	9.93	104.0
20H	22	2140	175.7–185.2	9.5	9.89	104.0
21H	22	2210	185.2–194.7	9.5	9.91	104.0
22H	22	2250	194.7–204.2	9.5	9.88	104.0
23H	22	2320	204.2–213.7	9.5	9.84	103.0
24H	22	2355	213.7–223.2	9.5	9.84	103.0
25H	22	0035	223.2–232.7	9.5	9.77	102.0
26H	23	0115	232.7–242.2	9.5	9.82	103.0
27H	23	0155	242.2–251.7	9.5	9.86	104.0
			Coring totals:	251.7	261.8	104.0
162-983C-						
1H	23	0430	0.0–3.9	3.9	3.89	99.7
2H	23	0505	3.9–13.4	9.5	9.83	103.0
3H	23	0540	13.4–22.9	9.5	9.85	103.0
4H	23	0615	22.9–32.4	9.5	9.99	105.0
5H	23	0650	32.4–41.9	9.5	9.95	105.0
6H	23	0730	41.9–51.4	9.5	10.03	105.6
7H	23	0810	51.4–60.9	9.5	10.02	105.5
8H	23	0845	60.9–70.4	9.5	9.89	104.0
9H	23	0920	70.4–79.9	9.5	9.61	101.0
10H	23	1000	79.9–89.4	9.5	10.02	105.5
11H	23	1035	89.4–98.9	9.5	10.04	105.7
12H	23	1115	98.9–108.4	9.5	9.92	104.0
13H	23	1150	108.4–117.9	9.5	9.92	104.0
14H	23	1230	117.9–127.4	9.5	10.03	105.6
15H	23	1310	127.4–136.9	9.5	9.92	104.0
16H	23	1340	136.9–146.4	9.5	9.92	104.0
17H	23	1415	146.4–155.9	9.5	10.02	105.5
18H	23	1450	155.9–165.4	9.5	9.95	105.0
19H	23	1520	165.4–174.9	9.5	9.98	105.0
20H	23	1555	174.9–184.4	9.5	10.02	105.5
21H	23	1625	184.4–193.9	9.5	9.71	102.0
22H	23	1655	193.9–203.4	9.5	10.00	105.2
23H	23	1730	203.4–212.9	9.5	9.83	103.0
24H	23	1810	212.9–222.4	9.5	9.80	103.0
25H	23	1840	222.4–231.9	9.5	9.90	104.0
26H	23	1910	231.9–241.4	9.5	9.98	105.0
27H	23	1950	241.4–250.9	9.5	9.78	103.0
28H	23	2025	250.9–260.4	9.5	9.95	105.0
			Coring totals:	260.4	271.8	104.4

Table 2. Site 983 composite depths.

Core, section	Length (cm)	Depth (mbsf)	Depth (mcd)	Offset (mcd – mbsf)
162-983A-				
1H-1	150	0.00	0.00	0.00
1H-2	150	1.50	1.50	0.00
1H-3	150	3.00	3.00	0.00
1H-4	150	4.50	4.50	0.00
1H-5	126	6.00	6.00	0.00
1H-CC	16	7.26	7.26	0.00
2H-1	150	7.40	8.59	1.19
2H-2	150	8.90	10.09	1.19
2H-3	150	10.40	11.59	1.19
2H-4	150	11.90	13.09	1.19
2H-5	150	13.40	14.59	1.19
2H-6	150	14.90	16.09	1.19
2H-7	70	16.40	17.59	1.19
2H-CC	21	17.10	18.29	1.19
3H-1	150	16.90	19.56	2.66
3H-2	150	18.40	21.06	2.66
3H-3	150	19.90	22.56	2.66
3H-4	150	21.40	24.06	2.66
3H-5	150	22.90	25.56	2.66
3H-6	150	24.40	27.06	2.66
3H-7	70	25.90	28.56	2.66
3H-CC	29	26.60	29.26	2.66
4H-1	150	26.40	30.36	3.96
4H-2	150	27.90	31.86	3.96
4H-3	150	29.40	33.36	3.96
4H-4	150	30.90	34.86	3.96
4H-5	150	32.40	36.36	3.96
4H-6	150	33.90	37.86	3.96
4H-7	79	35.40	39.36	3.96
4H-CC	18	36.19	40.15	3.96
5H-1	150	35.90	41.71	5.81
5H-2	150	37.40	43.21	5.81
5H-3	150	38.90	44.71	5.81
5H-4	150	40.40	46.21	5.81
5H-5	150	41.90	47.71	5.81
5H-6	150	43.40	49.21	5.81
5H-7	83	44.90	50.71	5.81
5H-CC	24	45.73	51.54	5.81
6H-1	150	45.40	51.36	5.96
6H-2	150	46.90	52.86	5.96
6H-3	150	48.40	54.36	5.96
6H-4	150	49.90	55.86	5.96
6H-5	150	51.40	57.36	5.96
6H-6	150	52.90	58.86	5.96
6H-7	79	54.40	60.36	5.96
6H-CC	19	55.19	61.15	5.96
7H-1	150	54.90	62.20	7.30
7H-2	150	56.40	63.70	7.30
7H-3	150	57.90	65.20	7.30
7H-4	150	59.40	66.70	7.30
7H-5	150	60.90	68.20	7.30
7H-6	150	62.40	69.70	7.30
7H-7	71	63.90	71.20	7.30
7H-CC	24	64.61	71.91	7.30
8H-1	150	64.40	72.27	7.87
8H-2	150	65.90	73.77	7.87
8H-3	150	67.40	75.27	7.87
8H-4	150	68.90	76.77	7.87
8H-5	150	70.40	78.27	7.87
8H-6	150	71.90	79.77	7.87
8H-7	67	73.40	81.27	7.87
8H-CC	26	74.07	81.94	7.87
9H-1	150	73.90	82.75	8.85
9H-2	150	75.40	84.25	8.85
9H-3	150	76.90	85.75	8.85
9H-4	150	78.40	87.25	8.85
9H-5	150	79.90	88.75	8.85
9H-6	150	81.40	90.25	8.85
9H-7	68	82.90	91.75	8.85
9H-CC	28	83.58	92.43	8.85
10H-1	150	83.40	92.74	9.34
10H-2	150	84.90	94.24	9.34
10H-3	150	86.40	95.74	9.34
10H-4	150	87.90	97.24	9.34
10H-5	150	89.40	98.74	9.34
10H-6	150	90.90	100.24	9.34
10H-7	67	92.40	101.74	9.34
10H-CC	25	93.07	102.41	9.34
11H-1	150	92.90	103.19	10.29
11H-2	150	94.40	104.69	10.29
11H-3	150	95.90	106.19	10.29
11H-4	150	97.40	107.69	10.29
11H-5	150	98.90	109.19	10.29
11H-6	150	100.40	110.69	10.29
11H-7	67	101.90	112.19	10.29
11H-CC	24	102.57	112.86	10.29
12H-1	150	102.40	113.22	10.82
12H-2	150	103.90	114.72	10.82
12H-3	150	105.40	116.22	10.82
12H-4	150	106.90	117.72	10.82
12H-5	150	108.40	119.22	10.82
12H-6	150	109.90	120.72	10.82
12H-7	74	111.40	122.22	10.82
12H-CC	24	112.14	122.96	10.82
13H-1	150	111.90	123.51	11.61
13H-2	150	113.40	125.01	11.61
13H-3	150	114.90	126.51	11.61
13H-4	150	116.40	128.01	11.61
13H-5	150	117.90	129.51	11.61
13H-6	150	119.40	131.01	11.61
13H-7	68	120.90	132.51	11.61
13H-CC	24	121.58	133.19	11.61
14H-1	150	121.40	133.71	12.31
14H-2	150	122.90	135.21	12.31
14H-3	150	124.40	136.71	12.31
14H-4	150	125.90	138.21	12.31
14H-5	150	127.40	139.71	12.31
14H-6	150	128.90	141.21	12.31
14H-7	69	130.40	142.71	12.31
14H-CC	26	131.09	143.40	12.31
15H-1	150	130.90	143.71	12.81
15H-2	150	132.40	145.21	12.81
15H-3	150	133.90	146.71	12.81
15H-4	150	135.40	148.21	12.81
15H-5	150	136.90	149.71	12.81
15H-6	150	138.40	151.21	12.81
15H-7	80	139.90	152.71	12.81
15H-CC	26	140.70	153.51	12.81
16H-1	150	140.40	154.30	13.90
16H-2	150	141.90	155.80	13.90
16H-3	150	143.40	157.30	13.90
16H-4	150	144.90	158.80	13.90
16H-5	150	146.40	160.30	13.90
16H-6	150	147.90	161.80	13.90
16H-7	64	149.40	163.30	13.90
16H-CC	23	150.04	163.94	13.90
17H-1	150	149.90	164.62	14.72
17H-2	150	151.40	166.12	14.72
17H-3	150	152.90	167.62	14.72
17H-4	150	154.40	169.12	14.72
17H-5	150	155.90	170.62	14.72
17H-6	150	157.40	172.12	14.72
17H-7	60	158.90	173.62	14.72
17H-CC	21	159.50	174.22	14.72
18H-1	150	159.40	175.08	15.68
18H-2	150	160.90	176.58	15.68
18H-3	150	162.40	178.08	15.68
18H-4	150	163.90	179.58	15.68
18H-5	150	165.40	181.08	15.68
18H-6	150	166.90	182.58	15.68
18H-7	66	168.40	184.08	15.68
18H-CC	25	169.06	184.74	15.68
19H-1	150	168.90	185.55	16.65
19H-2	150	170.40	187.05	16.65
19H-3	150	171.90	188.55	16.65
19H-4	150	173.40	190.05	16.65
19H-5	150	174.90	191.55	16.65
19H-6	150	176.40	193.05	16.65
19H-7	70	177.90	194.55	16.65
19H-CC	25	178.60	195.25	16.65
20H-1	150	178.40	195.83	17.43
20H-2	150	179.90	197.33	17.43
20H-3	150	181.40	198.83	17.43
20H-4	150	182.90	200.33	17.43
20H-5	150	184.40	201.83	17.43
20H-6	150	185.90	203.33	17.43
20H-7	68	187.40	204.83	17.43
20H-CC	22	188.08	205.51	17.43
21H-1	150	187.90	205.69	17.79
21H-2	150	189.40	207.19	17.79
21H-3	150	190.90	208.69	17.79
21H-4	150	192.40	210.19	17.79
21H-5	150	193.90	211.69	17.79
21H-6	150	195.40	213.19	17.79
21H-7	59	196.90	214.69	17.79
21H-CC	26	197.49	215.28	17.79
22H-1	150	197.40	216.44	19.04
22H-2	150	198.90	217.94	19.04
22H-3	150	200.40	219.44	19.04
22H-4	150	201.90	220.94	19.04
22H-5	150	203.40	222.44	19.04
22H-6	150	204.90	223.94	19.04
22H-7	66	206.40	225.44	19.04
22H-CC	2	207.06	226.10	19.04
23H-1	150	206.90	227.12	20.22
23H-2	150	208.40	228.62	20.22
23H-3	150	209.90	230.12	20.22

Table 2 (continued).

Core, section	Length (cm)	Depth (mbsf)	Depth (mcd)	Offset (mcd – mbsf)
23H-4	150	211.40	231.62	20.22
23H-5	150	212.90	233.12	20.22
23H-6	150	214.40	234.62	20.22
23H-7	60	215.90	236.12	20.22
23H-CC	20	216.50	236.72	20.22
24H-1	150	216.40	238.36	21.96
24H-2	150	217.90	239.86	21.96
24H-3	150	219.40	241.36	21.96
24H-4	150	220.90	242.86	21.96
24H-5	150	222.40	244.36	21.96
24H-6	150	223.90	245.86	21.96
24H-7	60	225.40	247.36	21.96
24H-CC	3	226.00	247.96	21.96
25H-1	150	225.90	248.71	22.81
25H-2	150	227.40	250.21	22.81
25H-3	150	228.90	251.71	22.81
25H-4	150	230.40	253.21	22.81
25H-5	150	231.90	254.71	22.81
25H-6	150	233.40	256.21	22.81
25H-7	40	234.90	257.71	22.81
25H-CC	17	235.30	258.11	22.81
26H-1	150	235.40	259.44	24.04
26H-2	150	236.90	260.94	24.04
26H-3	150	238.40	262.44	24.04
26H-4	150	239.90	263.94	24.04
26H-5	150	241.40	265.44	24.04
26H-6	150	242.90	266.94	24.04
26H-7	59	244.40	268.44	24.04
26H-CC	3	244.99	269.03	24.04
27H-1	150	244.90	269.59	24.69
27H-2	150	246.40	271.09	24.69
27H-3	150	247.90	272.59	24.69
27H-4	150	249.40	274.09	24.69
27H-5	150	250.90	275.59	24.69
27H-6	150	252.40	277.09	24.69
27H-7	64	253.90	278.59	24.69
27H-CC	27	254.54	279.23	24.69
162-983B-				
1H-1	150	0.00	0.00	0.00
1H-2	150	1.50	1.50	0.00
1H-3	150	3.00	3.00	0.00
1H-CC	23	4.50	4.50	0.00
2H-1	150	4.70	5.37	0.67
2H-2	150	6.20	6.87	0.67
2H-3	150	7.70	8.37	0.67
2H-4	150	9.20	9.87	0.67
2H-5	150	10.70	11.37	0.67
2H-6	150	12.20	12.87	0.67
2H-7	77	13.70	14.37	0.67
2H-CC	20	14.47	15.14	0.67
3H-1	150	14.20	16.09	1.89
3H-2	150	15.70	17.59	1.89
3H-3	150	17.20	19.09	1.89
3H-4	150	18.70	20.59	1.89
3H-5	150	20.20	22.09	1.89
3H-6	150	21.70	23.59	1.89
3H-7	84	23.20	25.09	1.89
3H-CC	19	24.04	25.93	1.89
4H-1	150	23.70	26.22	2.52
4H-2	150	25.20	27.72	2.52
4H-3	150	26.70	29.22	2.52
4H-4	150	28.20	30.72	2.52
4H-5	150	29.70	32.22	2.52
4H-6	150	31.20	33.72	2.52
4H-7	59	32.70	35.22	2.52
4H-CC	25	33.29	35.81	2.52
5H-1	150	33.20	36.63	3.43
5H-2	150	34.70	38.13	3.43
5H-3	150	36.20	39.63	3.43
5H-4	150	37.70	41.13	3.43
5H-5	150	39.20	42.63	3.43
5H-6	150	40.70	44.13	3.43
5H-7	71	42.20	45.63	3.43
5H-CC	18	42.91	46.34	3.43
6H-1	150	42.70	47.10	4.40
6H-2	150	44.20	48.60	4.40
6H-3	150	45.70	50.10	4.40
6H-4	150	47.20	51.60	4.40
6H-5	150	48.70	53.10	4.40
6H-6	150	50.20	54.60	4.40
6H-7	54	51.70	56.10	4.40
6H-CC	26	52.24	56.64	4.40
7H-1	150	52.20	57.18	4.98
7H-2	150	53.70	58.68	4.98
7H-3	150	55.20	60.18	4.98
7H-4	150	56.70	61.68	4.98
7H-5	150	58.20	63.18	4.98
7H-6	150	59.70	64.68	4.98
7H-7	71	61.20	66.18	4.98
7H-CC	23	61.91	66.89	4.98
8H-1	150	61.70	67.83	6.13
8H-2	150	63.20	69.33	6.13
8H-3	150	64.70	70.83	6.13
8H-4	150	66.20	72.33	6.13
8H-5	150	67.70	73.83	6.13
8H-6	150	69.20	75.33	6.13
8H-7	71	70.70	76.83	6.13
8H-CC	28	71.41	77.54	6.13
9H-1	150	71.20	78.38	7.18
9H-2	150	72.70	79.88	7.18
9H-3	150	74.20	81.38	7.18
9H-4	150	75.70	82.88	7.18
9H-5	150	77.20	84.38	7.18
9H-6	150	78.70	85.88	7.18
9H-7	83	80.20	87.38	7.18
9H-CC	25	81.03	88.21	7.18
10H-1	150	80.70	88.76	8.06
10H-2	150	82.20	90.26	8.06
10H-3	150	83.70	91.76	8.06
10H-4	150	85.20	93.26	8.06
10H-5	150	86.70	94.76	8.06
10H-6	150	88.20	96.26	8.06
10H-7	59	89.70	97.76	8.06
10H-CC	23	90.29	98.35	8.06
11H-1	150	90.20	98.93	8.73
11H-2	150	91.70	100.43	8.73
11H-3	150	93.20	101.93	8.73
11H-4	150	94.70	103.43	8.73
11H-5	150	96.20	104.93	8.73
11H-6	150	97.70	106.43	8.73
11H-7	73	99.20	107.93	8.73
11H-CC	29	99.93	108.66	8.73
12H-1	150	99.70	109.47	9.77
12H-2	150	101.20	110.97	9.77
12H-3	150	102.70	112.47	9.77
12H-4	150	104.20	113.97	9.77
12H-5	150	105.70	115.47	9.77
12H-6	150	107.20	116.97	9.77
12H-7	61	108.70	118.47	9.77
12H-CC	24	109.31	119.08	9.77
13H-1	150	109.20	119.69	10.49
13H-2	150	110.70	121.19	10.49
13H-3	150	112.20	122.69	10.49
13H-4	150	113.70	124.19	10.49
13H-5	150	115.20	125.69	10.49
13H-6	150	116.70	127.19	10.49
13H-7	70	118.20	128.69	10.49
13H-CC	10	118.90	129.39	10.49
14H-1	150	118.70	130.36	11.66
14H-2	150	120.20	131.86	11.66
14H-3	150	121.70	133.36	11.66
14H-4	150	123.20	134.86	11.66
14H-5	150	124.70	136.36	11.66
14H-6	150	126.20	137.86	11.66
14H-7	66	127.70	139.36	11.66
14H-CC	27	128.36	140.02	11.66
15H-1	150	128.20	140.65	12.45
15H-2	150	129.70	142.15	12.45
15H-3	150	131.20	143.65	12.45
15H-4	150	132.70	145.15	12.45
15H-5	150	134.20	146.65	12.45
15H-6	150	135.70	148.15	12.45
15H-7	75	137.20	149.65	12.45
15H-CC	27	137.95	150.40	12.45
16H-1	150	137.70	151.75	14.05
16H-2	150	139.20	153.25	14.05
16H-3	150	140.70	154.75	14.05
16H-4	150	142.20	156.25	14.05
16H-5	150	143.70	157.75	14.05
16H-6	150	145.20	159.25	14.05
16H-7	61	146.70	160.75	14.05
16H-CC	22	147.31	161.36	14.05
17H-1	150	147.20	161.54	14.34
17H-2	150	148.70	163.04	14.34
17H-3	150	150.20	164.54	14.34
17H-4	150	151.70	166.04	14.34
17H-5	150	153.20	167.54	14.34
17H-6	150	154.70	169.04	14.34
17H-7	68	156.20	170.54	14.34
17H-CC	26	156.88	171.22	14.34
18H-1	150	156.70	172.32	15.62
18H-2	150	158.20	173.82	15.62
18H-3	150	159.70	175.32	15.62
18H-4	150	161.20	176.82	15.62
18H-5	150	162.70	178.32	15.62
18H-6	150	164.20	179.82	15.62
18H-7	37	165.70	181.32	15.62

Table 2 (continued).

Core, section	Length (cm)	Depth (mbsf)	Depth (mcd)	Offset (mcd – mbsf)
18H-CC	24	166.07	181.69	15.62
19H-1	150	166.20	182.87	16.67
19H-2	150	167.70	184.37	16.67
19H-3	150	169.20	185.87	16.67
19H-4	150	170.70	187.37	16.67
19H-5	150	172.20	188.87	16.67
19H-6	150	173.70	190.37	16.67
19H-7	69	175.20	191.87	16.67
19H-CC	24	175.89	192.56	16.67
20H-1	150	175.70	193.04	17.34
20H-2	150	177.20	194.54	17.34
20H-3	150	178.70	196.04	17.34
20H-4	150	180.20	197.54	17.34
20H-5	150	181.70	199.04	17.34
20H-6	150	183.20	200.54	17.34
20H-7	65	184.70	202.04	17.34
20H-CC	24	185.35	202.69	17.34
21H-1	150	185.20	203.15	17.95
21H-2	150	186.70	204.65	17.95
21H-3	150	188.20	206.15	17.95
21H-4	150	189.70	207.65	17.95
21H-5	150	191.20	209.15	17.95
21H-6	150	192.70	210.65	17.95
21H-7	63	194.20	212.15	17.95
21H-CC	28	194.83	212.78	17.95
22H-1	150	194.70	213.37	18.67
22H-2	150	196.20	214.87	18.67
22H-3	150	197.70	216.37	18.67
22H-4	150	199.20	217.87	18.67
22H-5	150	200.70	219.37	18.67
22H-6	150	202.20	220.87	18.67
22H-7	64	203.70	222.37	18.67
22H-CC	24	204.34	223.01	18.67
23H-1	150	204.20	223.88	19.68
23H-2	150	205.70	225.38	19.68
23H-3	150	207.20	226.88	19.68
23H-4	150	208.70	228.38	19.68
23H-5	150	210.20	229.88	19.68
23H-6	150	211.70	231.38	19.68
23H-7	58	213.20	232.88	19.68
23H-CC	26	213.78	233.46	19.68
24H-1	150	213.70	234.13	20.43
24H-2	150	215.20	235.63	20.43
24H-3	150	216.70	237.13	20.43
24H-4	150	218.20	238.63	20.43
24H-5	150	219.70	240.13	20.43
24H-6	150	221.20	241.63	20.43
24H-7	61	222.70	243.13	20.43
24H-CC	23	223.31	243.74	20.43
25H-1	150	223.20	244.93	21.73
25H-2	150	224.70	246.43	21.73
25H-3	150	226.20	247.93	21.73
25H-4	150	227.70	249.43	21.73
25H-5	150	229.20	250.93	21.73
25H-6	150	230.70	252.43	21.73
25H-7	62	232.20	253.93	21.73
25H-CC	15	232.82	254.55	21.73
26H-1	150	232.70	255.21	22.51
26H-2	150	234.20	256.71	22.51
26H-3	150	235.70	258.21	22.51
26H-4	150	237.20	259.71	22.51
26H-5	150	238.70	261.21	22.51
26H-6	150	240.20	262.71	22.51
26H-7	63	241.70	264.21	22.51
26H-CC	19	242.33	264.84	22.51
27H-1	150	242.20	265.26	23.06
27H-2	150	243.70	266.76	23.06
27H-3	150	245.20	268.26	23.06
27H-4	150	246.70	269.76	23.06
27H-5	150	248.20	271.26	23.06
27H-6	150	249.70	272.76	23.06
27H-7	68	251.20	274.26	23.06
27H-CC	18	251.88	274.94	23.06
162-983C-				
1H-1	150	0.00	0.02	0.02
1H-2	150	1.50	1.52	0.02
1H-3	62	3.00	3.02	0.02
1H-CC	27	3.62	3.64	0.02
2H-1	150	3.90	5.25	1.35
2H-2	150	5.40	6.75	1.35
2H-3	150	6.90	8.25	1.35
2H-4	150	8.40	9.75	1.35
2H-5	150	9.90	11.25	1.35
2H-6	150	11.40	12.75	1.35
2H-7	68	12.90	14.25	1.35
2H-CC	15	13.58	14.93	1.35
3H-1	150	13.40	18.64	5.24
3H-2	150	14.90	20.14	5.24
3H-3	150	16.40	21.64	5.24
3H-4	150	17.90	23.14	5.24
3H-5	150	19.40	24.64	5.24
3H-6	150	20.90	26.14	5.24
3H-7	66	22.40	27.64	5.24
3H-CC	19	23.06	28.30	5.24
4H-1	150	22.90	28.06	5.16
4H-2	150	24.40	29.56	5.16
4H-3	150	25.90	31.06	5.16
4H-4	150	27.40	32.56	5.16
4H-5	150	28.90	34.06	5.16
4H-6	150	30.40	35.56	5.16
4H-7	80	31.90	37.06	5.16
4H-CC	19	32.70	37.86	5.16
5H-1	150	32.40	38.46	6.06
5H-2	150	33.90	39.96	6.06
5H-3	150	35.40	41.46	6.06
5H-4	150	36.90	42.96	6.06
5H-5	150	38.40	44.46	6.06
5H-6	150	39.90	45.96	6.06
5H-7	69	41.40	47.46	6.06
5H-CC	26	42.09	48.15	6.06
6H-1	150	41.90	49.80	7.90
6H-2	150	43.40	51.30	7.90
6H-3	150	44.90	52.80	7.90
6H-4	150	46.40	54.30	7.90
6H-5	150	47.90	55.80	7.90
6H-6	150	49.40	57.30	7.90
6H-7	80	50.90	58.80	7.90
6H-CC	23	51.70	59.60	7.90
7H-1	150	51.40	60.53	9.13
7H-2	150	52.90	62.03	9.13
7H-3	150	54.40	63.53	9.13
7H-4	150	55.90	65.03	9.13
7H-5	150	57.40	66.53	9.13
7H-6	150	58.90	68.03	9.13
7H-7	70	60.40	69.53	9.13
7H-CC	32	61.10	70.23	9.13
8H-1	150	60.90	71.19	10.29
8H-2	150	62.40	72.69	10.29
8H-3	150	63.90	74.19	10.29
8H-4	150	65.40	75.69	10.29
8H-5	150	66.90	77.19	10.29
8H-6	150	68.40	78.69	10.29
8H-7	64	69.90	80.19	10.29
8H-CC	25	70.54	80.83	10.29
9H-1	150	70.40	81.82	11.42
9H-2	150	71.90	83.32	11.42
9H-3	150	73.40	84.82	11.42
9H-4	150	74.90	86.32	11.42
9H-5	150	76.40	87.82	11.42
9H-6	150	77.90	89.32	11.42
9H-7	61	79.40	90.82	11.42
10H-1	150	79.90	91.03	11.13
10H-2	150	81.40	92.53	11.13
10H-3	150	82.90	94.03	11.13
10H-4	150	84.40	95.53	11.13
10H-5	150	85.90	97.03	11.13
10H-6	150	87.40	98.53	11.13
10H-7	72	88.90	100.03	11.13
10H-CC	30	89.62	100.75	11.13
11H-1	150	89.40	101.72	12.32
11H-2	150	90.90	103.22	12.32
11H-3	150	92.40	104.72	12.32
11H-4	150	93.90	106.22	12.32
11H-5	150	95.40	107.72	12.32
11H-6	150	96.90	109.22	12.32
11H-7	75	98.40	110.72	12.32
11H-CC	29	99.15	111.47	12.32
12H-1	150	98.90	112.23	13.33
12H-2	150	100.40	113.73	13.33
12H-3	150	101.90	115.23	13.33
12H-4	150	103.40	116.73	13.33
12H-5	150	104.90	118.23	13.33
12H-6	150	106.40	119.73	13.33
12H-7	67	107.90	121.23	13.33
12H-CC	25	108.57	121.90	13.33
13H-1	150	108.40	122.24	13.84
13H-2	150	109.90	123.74	13.84
13H-3	150	111.40	125.24	13.84
13H-4	150	112.90	126.74	13.84
13H-5	150	114.40	128.24	13.84
13H-6	150	115.90	129.74	13.84
13H-7	72	117.40	131.24	13.84
13H-CC	20	118.12	131.96	13.84
14H-1	150	117.90	132.33	14.43
14H-2	150	119.40	133.83	14.43
14H-3	150	120.90	135.33	14.43
14H-4	150	122.40	136.83	14.43

Table 2 (continued).

Core, section	Length (cm)	Depth (mbsf)	Depth (mcd)	Offset (mcd – mbsf)
14H-5	150	123.90	138.33	14.43
14H-6	150	125.40	139.83	14.43
14H-7	74	126.90	141.33	14.43
14H-CC	29	127.64	142.07	14.43
15H-1	150	127.40	142.72	15.32
15H-2	150	128.90	144.22	15.32
15H-3	150	130.40	145.72	15.32
15H-4	150	131.90	147.22	15.32
15H-5	150	133.40	148.72	15.32
15H-6	150	134.90	150.22	15.32
15H-7	63	136.40	151.72	15.32
15H-CC	29	137.03	152.35	15.32
16H-1	150	136.90	152.63	15.73
16H-2	150	138.40	154.13	15.73
16H-3	150	139.90	155.63	15.73
16H-4	150	141.40	157.13	15.73
16H-5	150	142.90	158.63	15.73
16H-6	150	144.40	160.13	15.73
16H-7	66	145.90	161.63	15.73
16H-CC	26	146.56	162.29	15.73
17H-1	150	146.40	162.91	16.51
17H-2	150	147.90	164.41	16.51
17H-3	150	149.40	165.91	16.51
17H-4	150	150.90	167.41	16.51
17H-5	150	152.40	168.91	16.51
17H-6	150	153.90	170.41	16.51
17H-7	75	155.40	171.91	16.51
17H-CC	27	156.15	172.66	16.51
18H-1	150	155.90	172.65	16.75
18H-2	150	157.40	174.15	16.75
18H-3	150	158.90	175.65	16.75
18H-4	150	160.40	177.15	16.75
18H-5	150	161.90	178.65	16.75
18H-6	150	163.40	180.15	16.75
18H-7	66	164.90	181.65	16.75
18H-CC	29	165.56	182.31	16.75
19H-1	150	165.40	183.42	18.02
19H-2	150	166.90	184.92	18.02
19H-3	150	168.40	186.42	18.02
19H-4	150	169.90	187.92	18.02
19H-5	150	171.40	189.42	18.02
19H-6	150	172.90	190.92	18.02
19H-7	76	174.40	192.42	18.02
19H-CC	22	175.16	193.18	18.02
20H-1	150	174.90	193.73	18.83
20H-2	150	176.40	195.23	18.83
20H-3	150	177.90	196.73	18.83
20H-4	150	179.40	198.23	18.83
20H-5	150	180.90	199.73	18.83
20H-6	150	182.40	201.23	18.83
20H-7	74	183.90	202.73	18.83
20H-CC	28	184.64	203.47	18.83
21H-1	150	184.40	203.85	19.45
21H-2	150	185.90	205.35	19.45
21H-3	150	187.40	206.85	19.45
21H-4	150	188.90	208.35	19.45
21H-5	150	190.40	209.85	19.45
21H-6	150	191.90	211.35	19.45
21H-7	57	193.40	212.85	19.45
21H-CC	14	193.97	213.42	19.45
22H-1	150	193.90	214.06	20.16
22H-2	150	195.40	215.56	20.16
22H-3	150	196.90	217.06	20.16
22H-4	150	198.40	218.56	20.16
22H-5	150	199.90	220.06	20.16
22H-6	150	201.40	221.56	20.16
22H-7	73	202.90	223.06	20.16
22H-CC	27	203.63	223.79	20.16
23H-1	150	203.40	224.33	20.93
23H-2	150	204.90	225.83	20.93
23H-3	150	206.40	227.33	20.93
23H-4	150	207.90	228.83	20.93
23H-5	150	209.40	230.33	20.93
23H-6	150	210.90	231.83	20.93
23H-7	64	212.40	233.33	20.93
23H-CC	19	213.04	233.97	20.93
24H-1	150	212.90	235.48	22.58
24H-2	150	214.40	236.98	22.58
24H-3	150	215.90	238.48	22.58
24H-4	150	217.40	239.98	22.58
24H-5	150	218.90	241.48	22.58
24H-6	150	220.40	242.98	22.58
24H-7	65	221.90	244.48	22.58
24H-CC	15	222.55	245.13	22.58
25H-1	150	222.40	246.28	23.88
25H-2	150	223.90	247.78	23.88
25H-3	150	225.40	249.28	23.88
25H-4	150	226.90	250.78	23.88
25H-5	150	228.40	252.28	23.88
25H-6	150	229.90	253.78	23.88
25H-7	64	231.40	255.28	23.88
25H-CC	26	232.04	255.92	23.88
26H-1	150	231.90	256.77	24.87
26H-2	150	233.40	258.27	24.87
26H-3	150	234.90	259.77	24.87
26H-4	150	236.40	261.27	24.87
26H-5	150	237.90	262.77	24.87
26H-6	150	239.40	264.27	24.87
26H-7	72	240.90	265.77	24.87
26H-CC	26	241.62	266.49	24.87
27H-1	150	241.40	267.88	26.48
27H-2	150	242.90	269.38	26.48
27H-3	150	244.40	270.88	26.48
27H-4	150	245.90	272.38	26.48
27H-5	150	247.40	273.88	26.48
27H-6	150	248.90	275.38	26.48
27H-7	62	250.40	276.88	26.48
27H-CC	16	251.02	277.50	26.48
28H-1	150	250.90	278.05	27.15
28H-2	150	252.40	279.55	27.15
28H-3	150	253.90	281.05	27.15
28H-4	150	255.40	282.55	27.15
28H-5	150	256.90	284.05	27.15
28H-6	150	258.40	285.55	27.15
28H-7	73	259.90	287.05	27.15
28H-CC	22	260.63	287.78	27.15

Note: Depths are from the top of each section.

(6) natural gamma-ray measurements, and (7) X-ray diffraction (XRD) analysis. No major lithologic boundaries occur within the 260 m of sediment recovered at this site. Subtle but distinct boundaries that demark three subunits occur at depths of 120 and 180 mbsf. The shallower boundary is recognized primarily in the spectral reflectance signal. It is characterized by a downcore decrease in the amplitude of the higher frequency (decimeter- to meter-scale) reflectance signal and an absence of the lower frequency reflectance signal (>10-m scale). The deeper boundary is recognized in visual examination of split cores and smear slides. It is characterized by a downcore absence of layers in which biocarbonate is predominant. All dropstones occur above this deeper horizon. Lithostratigraphic Unit I and its subunits are described in detail in the following section.

Description of Lithostratigraphic Unit

Unit I

Intervals:
Cores 162-983A-1H through 27H
Cores 162-983B-1H through 27H
Cores 162-983C-1H through 28H
Age: Holocene to late Pliocene
Depth: 0 to 260 mbsf

Unit I consists of three 60- to 120-m-thick subunits. Subunit IA occupies the uppermost 120 mbsf of Unit I, Subunit IB extends from 120 to 180 mbsf, and Subunit IC includes the lowermost sediments recovered, 180–260 mbsf (Table 4; Fig. 5). Unit I sediments are dominated by variable amounts of clay, silt, and calcareous nannofossils. Specifically, the unit consists of alternating intervals of two primary sets of lithofacies: (1) dark gray, dark greenish gray, very dark gray, and very dark greenish gray clay, silty clay, clayey silt, nannofossil clay, and clay with nannofossils, and (2) dark gray to very dark gray nannofossil clay mixed sediment, clayey nannofossil mixed sediment, and clayey mixed sediment with nannofossils. A third minor, more nannofossil-rich set of lithofacies occurs in Subunits IA and IB, and is absent in Subunit IC. It consists of light greenish gray, greenish gray, gray, dark gray, and dark greenish gray nannofossil ooze, nannofossil ooze with clay, nannofossil ooze with spicules, clayey nan-

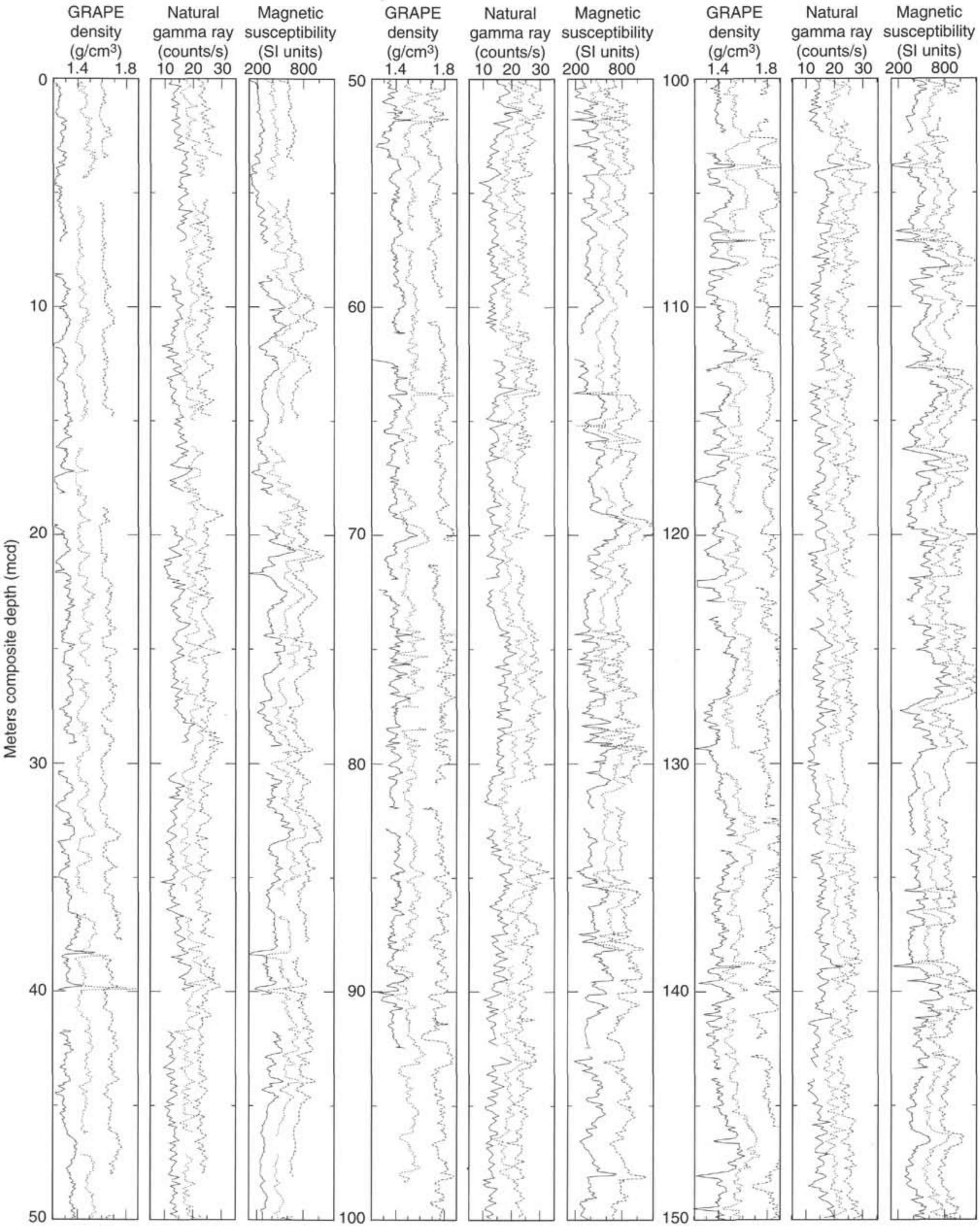

Figure 2. GRAPE density, natural gamma radiation, and magnetic susceptibility data from Site 983 on the mcd (meters composite depth) scale. Lines for Holes 983B (dotted) and 983C (dashed) have been horizontally offset from line for Hole 983A (solid) for better display; therefore, values given on horizontal scale are the true values only for Hole 983A. (See also back pocket.)

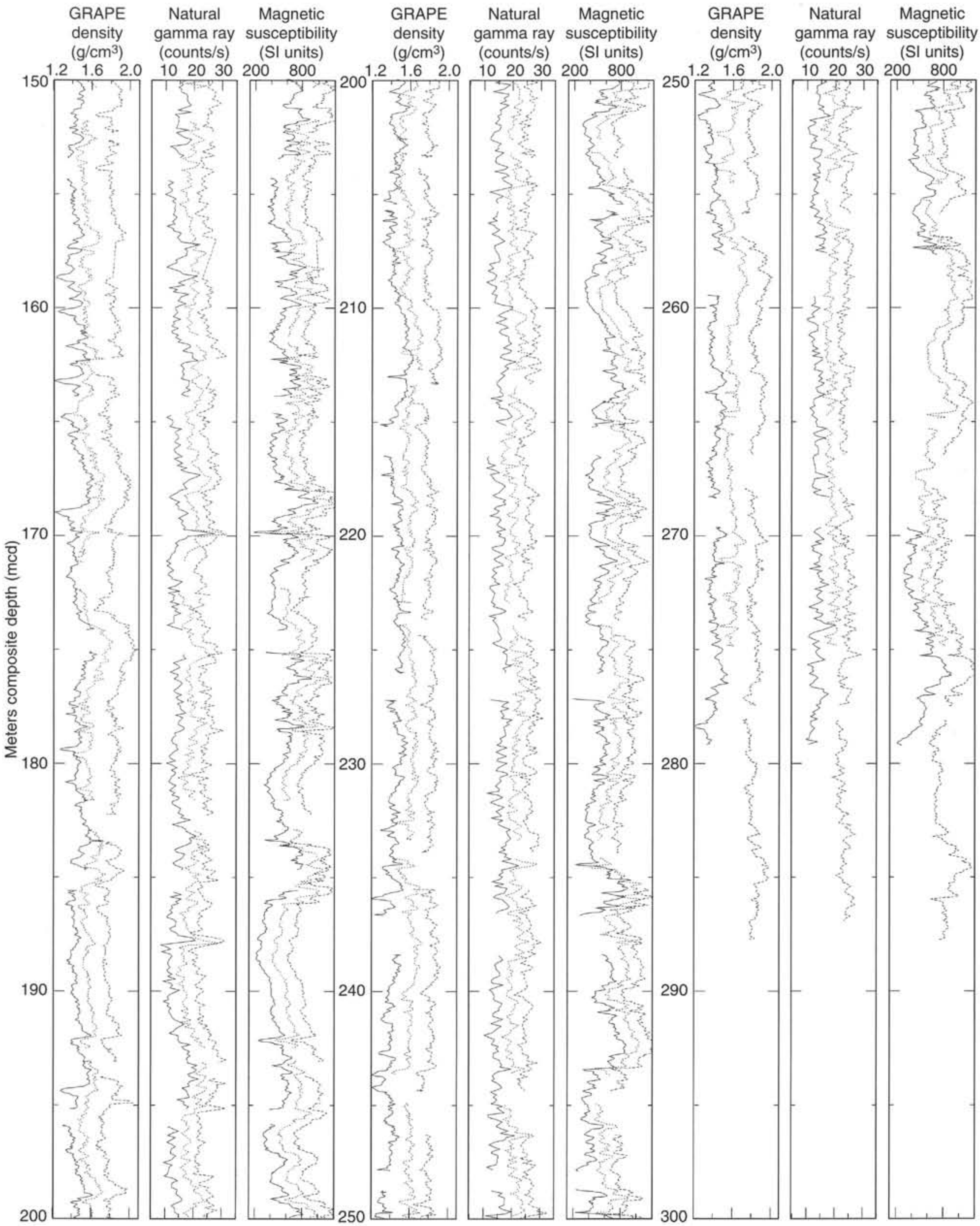

Figure 2 (continued).

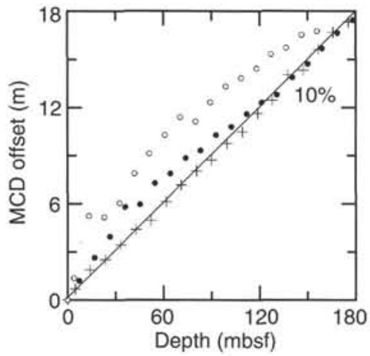

Figure 3. Depth offsets of the Site 983 meters composite depth scale relative to mbsf depth, illustrating the "growth" of the composite depth scale. Solid circles = Hole 983A, crosses = Hole 983B, open circles = Hole 983C.

Table 3. Site 983 splice tie points.

Hole, core, section (cm)	Depth (mbsf)	Depth (mcd)		Hole, core, section (cm)	Depth (mbsf)	Depth (mcd)
162-983-				162-983-		
A-1H-5, 53	6.53	6.53	tie to	B-2H-1, 116	5.86	6.53
B-2H-2, 62	6.82	7.49	tie to	C-2H-2, 74	6.14	7.49
C-2H-5, 104	10.94	12.29	tie to	A-2H-3, 71	11.10	12.29
A-2H-7, 8	16.48	17.67	tie to	B-3H-2, 8	15.78	17.67
B-3H-3, 137	18.57	20.46	tie to	C-3H-2, 32	15.22	20.46
C-3H-6, 146	22.35	27.59	tie to	B-4H-1, 137	25.07	27.59
B-4H-3, 29	26.99	29.51	tie to	C-4H-1, 146	24.35	29.51
C-4H-5, 128	30.17	35.33	tie to	A-4H-4, 47	31.37	35.33
A-4H-7, 53	35.93	39.89	tie to	C-5H-1, 143	33.83	39.89
C-5H-4, 134	38.24	44.30	tie to	A-5H-2, 109	38.49	44.30
A-5H-7, 5	44.94	50.75	tie to	C-6H-1, 95	42.85	50.75
C-6H-6, 124	50.64	58.54	tie to	B-7H-1, 136	53.56	58.54
B-7H-4, 136	58.06	63.04	tie to	C-7H-2, 101	53.91	63.04
C-7H-7, 17	60.57	69.70	tie to	B-8H-2, 37	63.57	69.70
B-8H-3, 131	66.01	72.14	tie to	C-8H-1, 95	61.85	72.04
C-8H-6, 47	68.86	79.15	tie to	B-9H-1, 77	71.97	79.15
B-9H-5, 20	77.39	84.57	tie to	C-9H-2, 125	73.15	84.57
C-9H-6, 125	79.15	90.57	tie to	B-10H-2, 32	82.51	90.57
B-10H-3, 115	84.85	92.91	tie to	C-10H-2, 38	81.78	92.91
C-10H-7, 44	89.34	100.47	tie to	B-11H-2, 5	91.74	100.47
B-11H-4, 25	94.95	103.68	tie to	C-11H-2, 46	91.36	103.68
C-11H-6, 68	97.58	109.90	tie to	B-12H-1, 44	100.13	109.90
B-12H-3, 64	103.34	113.11	tie to	C-12H-1, 88	99.78	113.11
C-12H-6, 97	107.37	120.70	tie to	B-13H-1, 101	110.24	120.70
B-13H-3, 32	112.51	123.00	tie to	C-13H-1, 76	109.16	123.00
C-13H-5, 20	114.60	128.44	tie to	A-13H-4, 44	116.83	128.44
A-13H-6, 8	119.48	131.09	tie to	B-14H-1, 74	119.43	131.09
B-14H-3, 43	122.13	133.79	tie to	C-14H-1, 146	119.36	133.79
C-14H-6, 107	126.47	140.90	tie to	B-15H-1, 25	128.45	140.90
B-15H-3, 14	131.33	143.78	tie to	C-15H-1, 106	128.46	143.78
C-15H-5, 113	134.52	149.84	tie to	A-15H-5, 13	137.03	149.84
A-15H-7, 56	140.46	153.27	tie to	C-16H-1, 65	137.54	153.27
C-16H-2, 146	139.85	155.58	tie to	A-16H-1, 128	141.68	155.58
A-16H-7, 32	149.71	163.61	tie to	C-17H-1, 71	147.10	163.61
C-17H-5, 130	153.70	170.21	tie to	A-17H-4, 109	155.49	170.21
A-17H-7, 38	159.27	173.99	tie to	C-18H-1, 134	157.24	173.99
C-18H-6, 83	164.22	180.97	tie to	A-18H-4, 140	165.29	180.97
A-18H-6, 134	168.24	183.92	tie to	C-19H-1, 50	165.90	183.92
C-19H-6, 128	174.17	192.19	tie to	A-19H-5, 64	175.54	192.19
A-19H-6, 56	176.95	193.60	tie to	B-20H-1, 56	176.26	193.60
B-20H-2, 64	177.84	195.18	tie to	C-20H-1, 145	176.35	195.18
C-20H-7, 16	184.06	202.89	tie to	A-20H-5, 107	185.46	202.89
A-20H-7, 17	187.57	205.00	tie to	C-21H-1, 115	185.55	205.00
C-21H-6, 146	193.36	212.81	tie to	A-21H-5, 113	195.02	212.81
A-21H-7, 35	197.25	215.04	tie to	C-22H-1, 98	194.88	215.04
C-22H-6, 41	201.81	221.97	tie to	A-22H-4, 104	202.93	221.97
A-22H-6, 143	206.32	225.36	tie to	C-23H-1, 103	204.43	225.36
C-23H-6, 89	211.78	232.71	tie to	A-23H-4, 110	212.49	232.71
A-23H-6, 124	215.64	235.86	tie to	C-24H-1, 38	213.28	235.86
C-24H-6, 104	221.43	244.01	tie to	A-24H-4, 116	222.05	244.01
A-24H-5, 125	223.65	245.61	tie to	B-25H-1, 68	223.88	245.61
B-25H-2, 85	225.55	247.28	tie to	C-25H-1, 100	223.40	247.28
C-25H-6, 106	230.96	254.84	tie to	A-25H-5, 14	232.03	254.84
A-25H-6, 100	234.40	257.21	tie to	C-26H-1, 44	232.34	257.21
C-26H-5, 136	239.26	264.13	tie to	A-26H-4, 19	240.09	264.13
A-26H-6, 52	243.42	267.46	tie to	B-27H-2, 71	244.40	267.46
B-27H-4, 44	247.14	270.20	tie to	C-27H-2, 82	243.72	270.20
C-27H-7, 8	250.47	276.95	tie to	A-27H-5, 136	252.26	276.95
A-27H-6, 124	253.64	278.33	tie to	C-28H-1, 29	251.18	278.33
C-28H-7, 68	260.58	287.73				

nofossil ooze, and clayey nannofossil ooze with spicules. XRD and smear slide analyses reveal that quartz and feldspar dominate the detrital silt component found in the silty dark gray clay layers, while tachylyte, amphiboles, pyroxenes, micas, and inorganic calcite are lesser constituents.

The mean carbonate content of Unit I is 16.4%, as measured in Hole 983A (Fig. 6; see "Organic Geochemistry" section, this chapter). Values fluctuate from 1.7% at 208.30 mbsf to 42.4% at 8.03 mbsf. The relatively high-amplitude 10-m-scale variations in carbonate content are superimposed on a longer trend of diminishing values downcore, which is most noticeable in Subunit IA.

The spectral reflectance signal in Site 983 sediments is remarkably diminished compared to previous sites, with few peaks above 20% (Figs. 5, 6; compare to "Site 980/981" and "Site 982" chapters, this volume). Values for reflectance within the red band (650–700 nm) for Subunit IA average 10%, and deviate 4%–5% above and below the average reflectance. Toward the base of Subunit IA, the values diminish to an average of 6%. With few exceptions (e.g., 159–162 mbsf and 170–176 mbsf), the reflectance across all spectral bands remains low. Downcore, through Subunits IB and IC, the percentage reflectance within the red band seldom deviates from 6%.

Dropstones are uncommon at Site 983, averaging fewer than four per hole. Eleven dropstones between 1 cm and 5 cm in size (Fig. 7) were identified throughout Subunits IA and IB, and none were identified in Subunit IC (Fig. 5). They occur in the more common dark-colored, clay-rich intervals. The distribution, texture, and composition of all dropstones greater than 1 cm in size are summarized in Table 5.

Scattered thin ash layers and ash pods occur throughout Unit I. A single 8-cm-thick (rhyolitic?) ash bed is evident within Subunit IB in all three holes (Fig. 8).

There is no evidence of significant sediment disturbance by natural processes at Site 983. Visible bedding planes and color contacts are horizontal and parallel, with no erosional relief, although most are mottled by bioturbation (Fig. 9). Bioturbation is ubiquitous throughout the cores, and is characterized by discrete burrows, blurred transitions, and fine-scale mottling.

Interpretation

Sediments accumulating at Site 983 include terrigenous and biogenic components. Both calcium carbonate and siliceous microfossils are well preserved throughout the recovered sequence (see "Biostratigraphy" section, this chapter) and there is no sedimentological evidence for erosion or winnowing. Consequently, changes in relative proportions of these two sediment types must reflect variable deposition rates rather than selective sediment removal. The maintenance of higher-than-typical sedimentation rates (100–150 m/m.y.), dominated by fine-grained clastics, throughout the late Pliocene and Pleistocene may be related to local surface water and atmospheric effects such as dust plumes or sea-ice melting, but is more likely due to deep-sea sediment focusing at this site (McCave and Tucholke, 1986). The low sand content (3%–5%) and paucity of dropstones, on the other hand, indicate the occurrence but relatively limited influence of ice-rafting as a depositional mechanism during this same interval.

The biogenic component of sediments at Site 983, as observed in smear slides, consists primarily of calcareous nannofossils. Bulk carbonate values peak at ~40%, lower than peak values for the same time interval at Sites 980, 981, and 982. This may reflect diminished productivity and/or enhanced dilution by the high terrigenous sedimentation rates at this site. Diminished terrigenous sediment input would explain both the general increasing trend in carbonate content upsection and somewhat decreased overall sedimentation rate within Subunit IA (see "Sedimentation Rates" section, this chapter). Varying dilution might also account for the slight covariance of calcareous

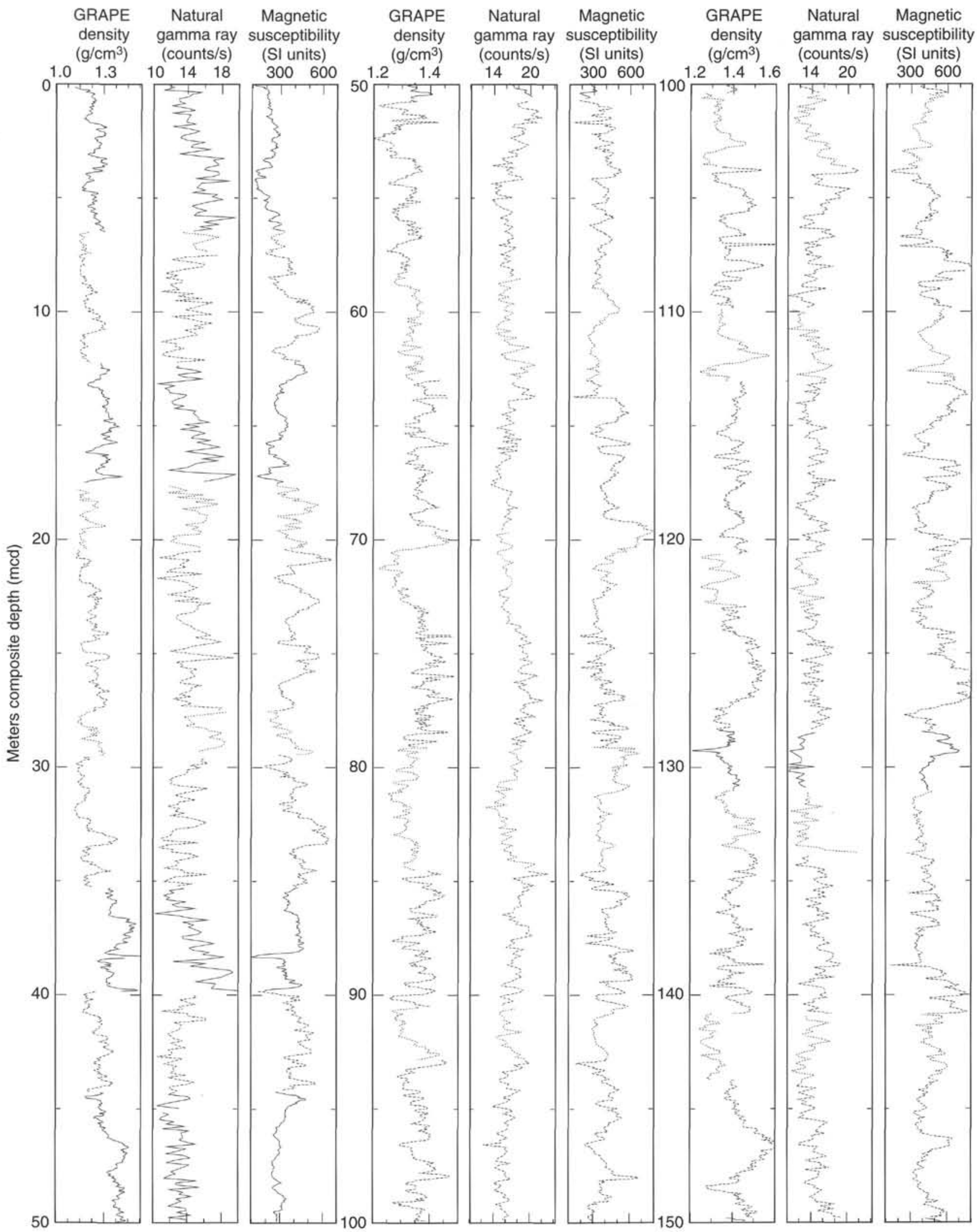

Figure 4. Spliced records of GRAPE density, natural gamma radiation, and magnetic susceptibility data from Site 983. Tie points for forming the splice are given in Table 3. Holes are 983A (solid line), 983B (dotted line), and 983C (dashed line).

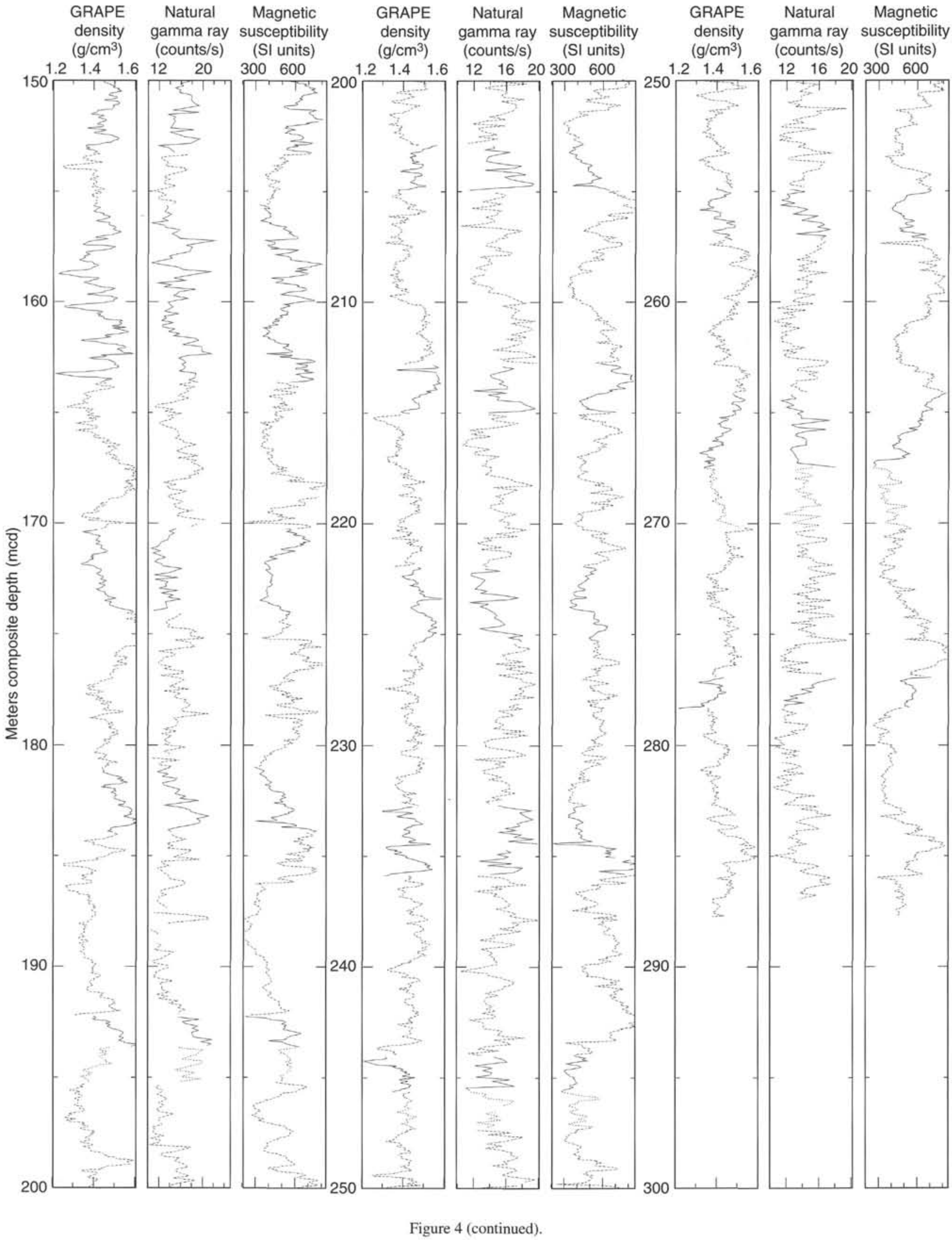

Figure 4 (continued).

Table 4. Summary table of sediment characteristics found in lithostratigraphic Unit I at Site 983.

Unit	Subunit	Depth (mbsf)	Thickness (m)	Age	Dominant lithologies/criteria	Calcium carbonate (%) Avg.	Min.	Max.
I		0–260.2	260.2	Pleist.–late Plio.	Cyclic (0.5 to 10 m) lithologic changes	16.4	1.7	42.4
	IA	0–120.0	120.0	Pleistocene	Clay, silty clay, clayey silt, clayey nannofossil mixed sediment nannofossil ooze, nannofossil clay/cyclic lithologic changes, terrigeneous and biogenic components often nearly equal, variable color			
	IB	120.0–180.0	60.0	Pleistocene	Clay, silty clay, clayey silt, clayey nannofossil mixed sediment, nannofossil ooze, nannofossil clay/cyclic lithologic changes, terrigeneous and biogenic components often nearly equal, invariant color			
	IC	180.0–260.2	80.2	Pleist.–late Plio.	Clay, silty clay, clayey silt/cyclic lithologic changes, terrigeneous components dominant, invariant color			

and siliceous microfossil abundance, although this might also reflect environmental influences on productivity. It is interesting to note the carbonate minimum from 130 to 160 mbsf (1.1–1.4 Ma) at Site 983 is approximately equivalent in time to a minimum carbonate interval observed in sediments recovered from the Nordic Seas during Legs 104 and 151 (Baumann et al., unpubl. data).

The carbonate content of Site 983 sediments appears to influence spectral reflectance even at low concentrations, although values observed at this site fall on the portion of the curvilinear reflectance/carbonate relationship where spectral reflectance seems somewhat less sensitive to carbonate content (fig. 9, "Site 984" chapter, this volume). Noncarbonate sediment components appear to influence the magnetic susceptibility and natural gamma radiation records at Site 983, as the two vary independently of reflectance, and appear to move in and out of phase with each other. Both signals fluctuate at depth scales that approximate orbital periodicities, varying from eccentricity to obliquity band (see "Sedimentation Rates" section, this chapter) as well as suborbital time scales. The spectral reflectance variations are greatest in Subunit IA, where relatively large changes occur with a period of approximately 40 m.

BIOSTRATIGRAPHY

A continuous sequence of sediments ranging in age from late Pliocene to Holocene (2.0 to 0 Ma) was recovered at Site 983, located on the Gardar Drift on the eastern flank of the Reykjanes Ridge. Calcareous nannofossils are the dominant fossil group at this site. However, all fossil groups exhibit variable abundance and preservation, possibly correlated to glacial/interglacial events. Biostratigraphic zonations for all microfossil groups are summarized in Figure 10.

Age information, with the exception of the occurrence of the diatom *N. fossilis* in sediment younger than expected, indicates that the Site 983 sedimentary sequence is continuous, without significant hiatuses. Age boundaries at this site are based on nannofossil data (Fig. 10). Sedimentation rates were determined using magnetic polarity data combined with the biostratigraphic datums presented in Table 6. For a detailed discussion of sedimentation rates at Site 983, see the "Sedimentation Rates" section (this chapter).

Calcareous Nannofossils

Calcareous nannofossils are generally abundant and well preserved at Site 983. However, a number of samples from various stratigraphic levels yielded rare and poorly preserved nannofossils. Commonly, Cretaceous nannofossils are present in these intervals. Most of these Cretaceous nannofossils are likely to be ice-rafted from the North Sea area, which is the highest latitude area in the North Atlantic that contains abundant Cretaceous nannofossils (see detailed discussion by Donnally, 1989). Nannofossil assemblages recovered from Site 983 are similar to those from previous sites, with relatively low species diversities and a general dominance of *Gephyrocapsa.* Other than the Cretaceous nannofossils in a number of samples as mentioned above, reworking of older fossils into younger sediment is minimal or undetectable. All the standard Pleistocene nannofossil zones are recognizable (Fig. 10). Nannofossil zonal boundaries, as well as some nontraditional markers, are summarized in Table 6.

Planktonic Foraminifers

Planktonic foraminifers are generally common to abundant and well preserved throughout the latest Pliocene to Holocene sequence in Hole 983A. A single barren interval is found in Sample 162-983A-16H-CC. Planktonic foraminifers are frequently dominated by *Neogloboquadrina pachyderma* (sinistrally coiling variety) but also include *Globigerina bulloides, Globorotalia inflata, Globorotalia scitula, Globigerinita glutinata, Globigerina quinqueloba,* and *N. pachyderma* (dextrally coiling variety). Assemblages dominated by *N. pachyderma* (sinistrally coiling) are inferred to reflect glacial conditions, while assemblages with abundant *Gg. bulloides, Gr. inflata,* and *N. pachyderma* (dextrally coiling variety) are inferred to reflect interglacial conditions. Assemblage composition is dependent upon whether the core-catcher sample chanced to fall within an interglacial or glacial interval. Subpolar paleoenvironmental conditions are indicated throughout the sequence. The start of the acme zone of *N. pachyderma* (sinistrally coiling), between Samples 162-983A-25H-2, 20 cm, and 5H-4, 20 cm, falls just below the base of the Pleistocene (Fig. 10).

Benthic Foraminifers

Benthic foraminifers are present at most of the levels examined, although the lowermost samples from Site 983 exhibit more impoverished benthic faunas than the overlying late Pleistocene sequence. A single barren interval is recorded in Sample 162-983A-16H-CC. Diversity is highly variable, but generally low below Sample 162-983A-18H-CC. Preservation is good throughout, although it is notable that the aragonitic species *Hoeglundina elegans* only occurs below Sample 162-983A-24H-CC.

The most common taxa include *Cassidulina teretis, Cibicidoides wuellerstorfi, Epistominella exigua, Melonis* spp., *Pullenia* spp., *Pyrgo* spp., and *Stainforthia* spp. The relative abundances of these taxa are variable, presumably in response to inferred glacial/interglacial cycles. The last occurrence of *Stilostomella lepidula* in Sample 162-983A-15H-CC represents the only significant biostratigraphic event. Falling at an interpolated age of 1.22 Ma, this LO appears to occur earlier here than at Sites 980, 981, and 982. There is no published age for this datum. (For further discussion, see "Biostratigraphy" section, "Sites 980/981" chapter, this volume.)

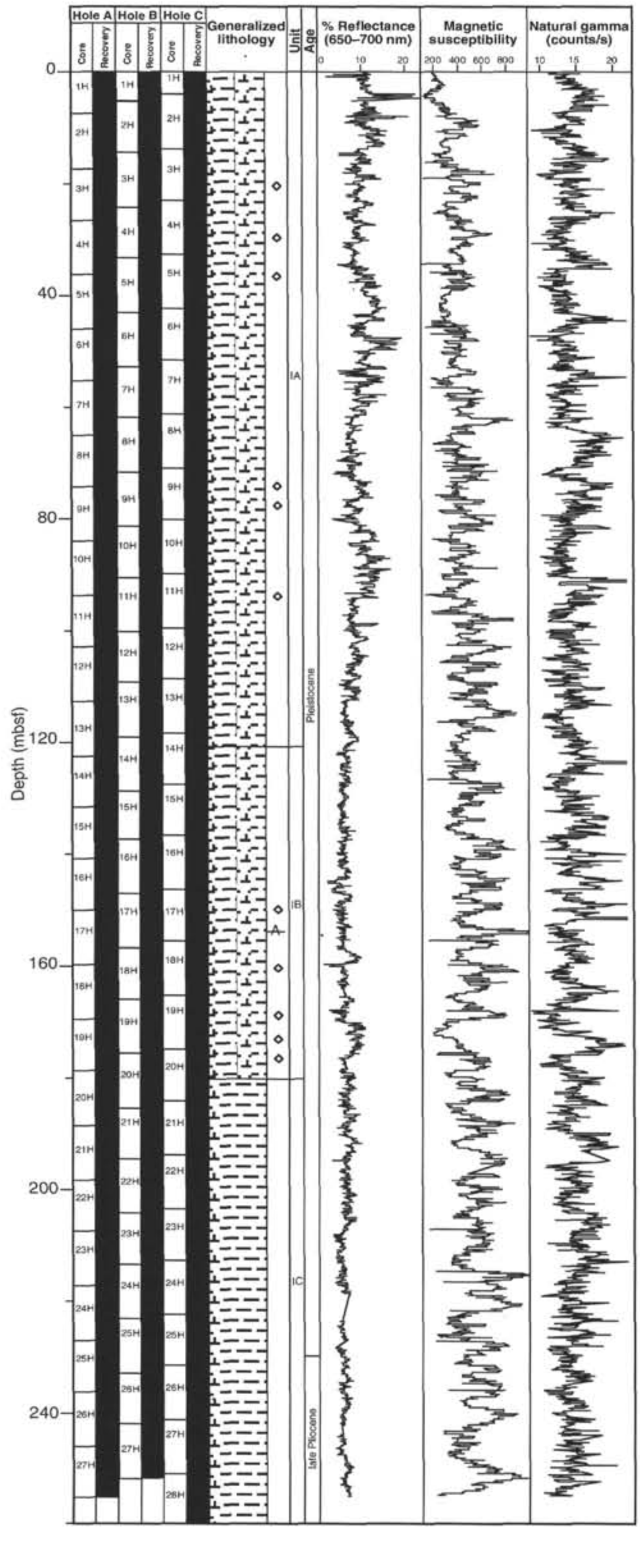

Figure 5. Core recovery, lithostratigraphy, age, spectral reflectance (red band), magnetic susceptibility, and natural gamma radiation of sediments recovered in Holes 983A, 983B, and 983C. Locations of dropstones (open diamonds) are shown in the column adjacent to the lithostratigraphy. Percentage reflectance, magnetic susceptibility, and natural gamma radiation records are from Hole 983A. (Key to symbols used in the "Generalized Lithology" column can be found in fig. 4, "Explanatory Notes" chapter, this volume.)

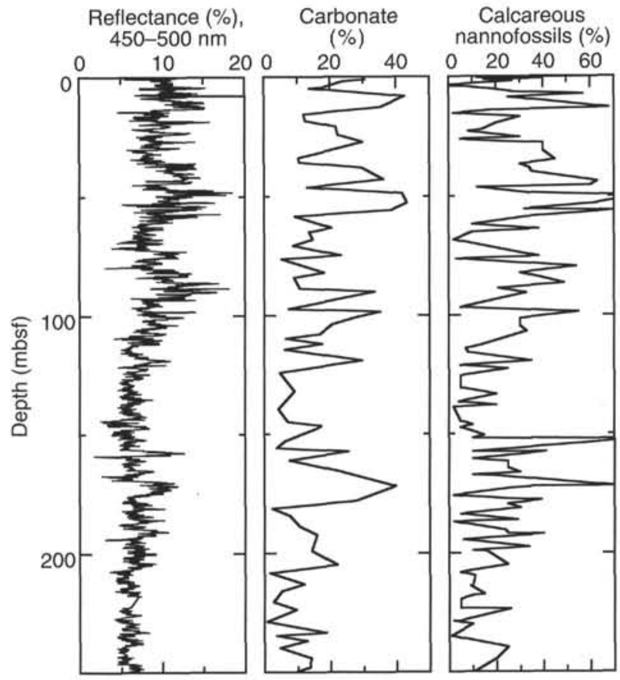

Figure 6. Spectral reflectance (blue band), bulk carbonate content, and calcareous nannofossil content of sediments recovered from Holes 983A, 983B, and 983C. Carbonate content and spectral reflectance records are from Hole 983A.

Diatoms

Diatoms were common to abundant throughout the Site 983 sequence and exhibited moderate to good preservation. This allowed the determination of several diatoms' first and last occurrences. Due to possible cold-water influences, species such as *Nitzschia reinholdii* and *Pseudoeunotia doliolus,* which are important late Pleistocene markers in the North Atlantic, were rare. Occurrences of many cooler-water indicators, such as *Neodenticula seminae* and *Rhizosolenia curvirostris,* were more common. The first and last occurrences of *Rhizosolenia curvirostris,* the last occurrence of *Nitzschia reinholdii,* and the first occurrence of *Pseudoeunotia doliolus* were reliable datums for the Site 983 sedimentary sequence. The presence of *Nitzschia fossilis* in sediments younger than its expected last occurrence suggests that sediment reworking may have occurred.

Siliceous Flagellates

Siliceous flagellates (including silicoflagellates, ebridians, and actiniscidians) are present between Samples 162-983A-3H-CC and 27H-CC, with abundances ranging from trace to common. Preservation of silicoflagellates is usually moderate, while preservation of actiniscidians and ebridians is good.

Silicoflagellates

Below a barren interval, Samples 162-983A-3H-CC to 26H-CC can be placed in the *Distephanus speculum* Zone, which is Holocene to latest Pliocene in age. The *Mesocena quadrangula* Subzone occurs from Sample 162-983A-9H-CC to 11H-CC, with an upper age of 0.83 Ma. The lowermost Sample 162-983A-27H-CC belongs to the upper Pliocene part of the *Distephanus aculeatus* Zone.

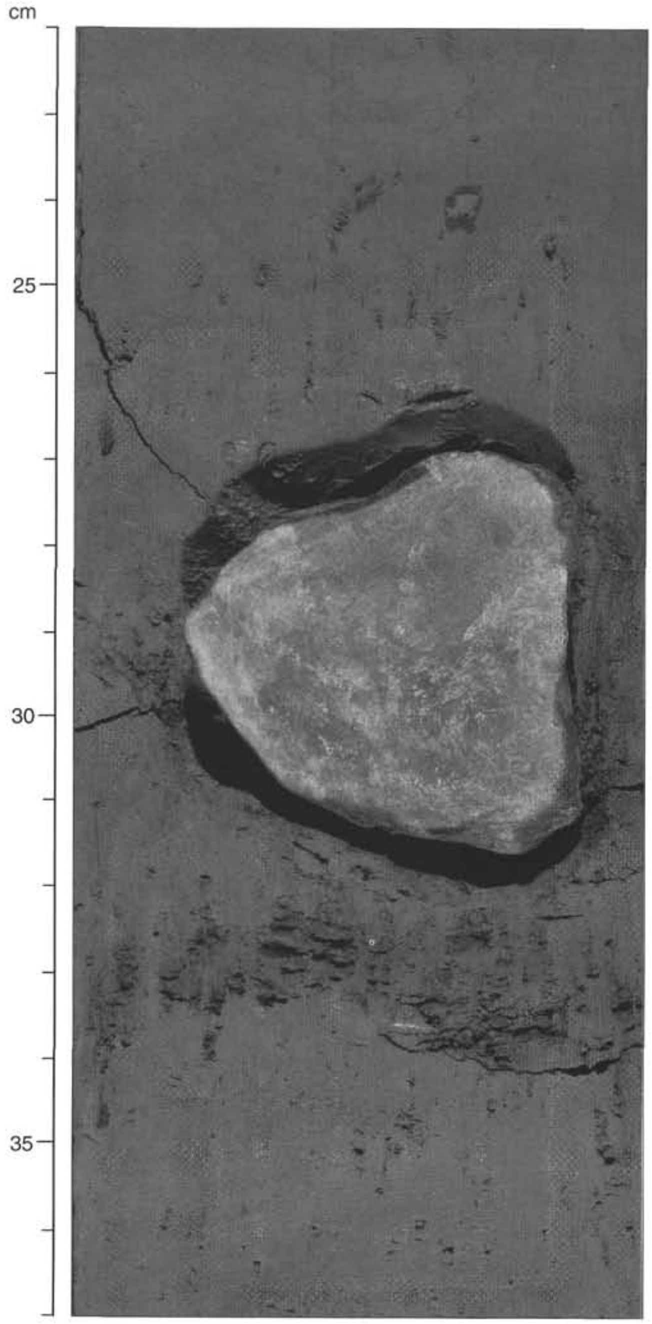

Figure 7. Photograph of a 5-cm angular crystalline dropstone found in Section 162-983B-5H-3, 22–37 cm.

Actiniscidians and Ebridians

Below a barren interval, Samples 162-983A-3H-CC to 26H-CC are assigned to the *Actiniscus pentasterias* Zone. The lowermost Sample 162-983A-27H-CC is attributed to the *Ammodochium serotinum* Zone of late Pliocene age, with an upper age of 2.0 Ma.

PALEOMAGNETISM

At Site 983, all archive halves of Holes 983A, 983B, and 983C were measured using the pass-through cryogenic magnetometer with a 5-cm measurement interval. Demagnetization was carried out at peak alternating fields of 25 mT for all core sections. Additional demagnetization at 30 mT was carried out on some core sections, as time allowed (Table 7). At the 25-mT demagnetization level, magnetization intensities fluctuate around 150 mA/m. Large variations in magnetic intensity are observed close to polarity reversals, where intensities often decrease to about 10 mA/m.

Table 5. Summary table of dropstones greater than 1 cm in size found at Site 983.

Core, section, interval top (cm)	Depth (mbsf)	Size (cm)	Composition	Shape
162-983A-				
3H-4, 41	21.8	1.0	Black, basalt	Subrounded
4H-6, 68	35.7	1.2	Black, soft, mudstone	Subangular
162-983B-				
5H-3, 26	39.2	5.0	Basalt	Subrounded
11H-4, 34	95.1	4.0	Felsic igneous	Rounded
18H-4, 51	161.7	1.5	Igneous	Subangular
19H-7, 30	175.5	1.0	Igneous	Angular
162-983C-				
9H-3, 19	73.6	1.0	Basalt	Subrounded
9H-4, 143	76.3	2.0	Basalt	Subrounded
17H-3, 51	149.5	1.5	Sandstone	Subangular
19H-7, 13	174.5	2.5	Black	Subangular
20H-1, 110	176.0	7.5	Diorite	Subangular

Discrete-sample stepwise AF demagnetization indicates that the steeply inclined drill-string (viscous) magnetization was removed by demagnetization fields exceeding 10 mT (Fig. 11). In some cores, the upper 25%–50% of Section 1 appears to have a high coercivity (drill-string) remagnetization which was not removed at peak alternating fields of 25 or 30 mT.

The Brunhes/Matuyama boundary, the Jaramillo Subchron, and the top of the Olduvai Subchron are well defined in all three holes (Fig. 12). Subbottom depths of polarity chron boundaries are given in Table 8. The base of the Olduvai Subchron is observed only in Hole 983C. A prominent normal-polarity subchron observed in all three holes between the Jaramillo and Olduvai Subchrons is tentatively identified as the Cobb Mountain Subchron.

A thin interval within the Brunhes Chron of low negative inclinations, close to 20 mbsf (Fig. 12), occurs in all three holes and may represent a magnetic excursion within the Brunhes Chron. Thin intervals of low positive inclinations within the Matuyama Chron, some of which are present in all three holes (for example, close to 125 mbsf and near 190 mbsf), may represent magnetic events within the Matuyama Chron or intervals in which the steep downward drill-string remagnetization has not been completely removed.

The high fidelity of the magnetic polarity stratigraphy and the high sedimentation rates (~11–13 cm/k.y.) bode well for the possibility of high-resolution polarity transition records at this site. Transitional directions are recorded over 50–150 cm of core at most polarity zone boundaries; however, some may be artifacts of the NRM acquisition process.

Trial normalizations of NRM intensity records (after demagnetization at 25 mT) by MST volume susceptibility produce coherent "paleointensity" records which do not appear to co-vary with susceptibility and correlate among the three holes. The potential of the above will be explored by high-resolution shore-based studies.

SEDIMENTATION RATES

A sedimentary section 260 m thick was recovered at Site 983, extending to the late Pliocene. Sedimentation rate reconstructions were based on magnetic polarity events from all three holes and calcareous nannofossil datums from Hole 983A (see "Paleomagnetism" and "Biostratigraphy" sections, this chapter). The Site 983 composite depth section (see "Composite Depths" section, this chapter) was used to relate events recorded in multiple holes to a common depth

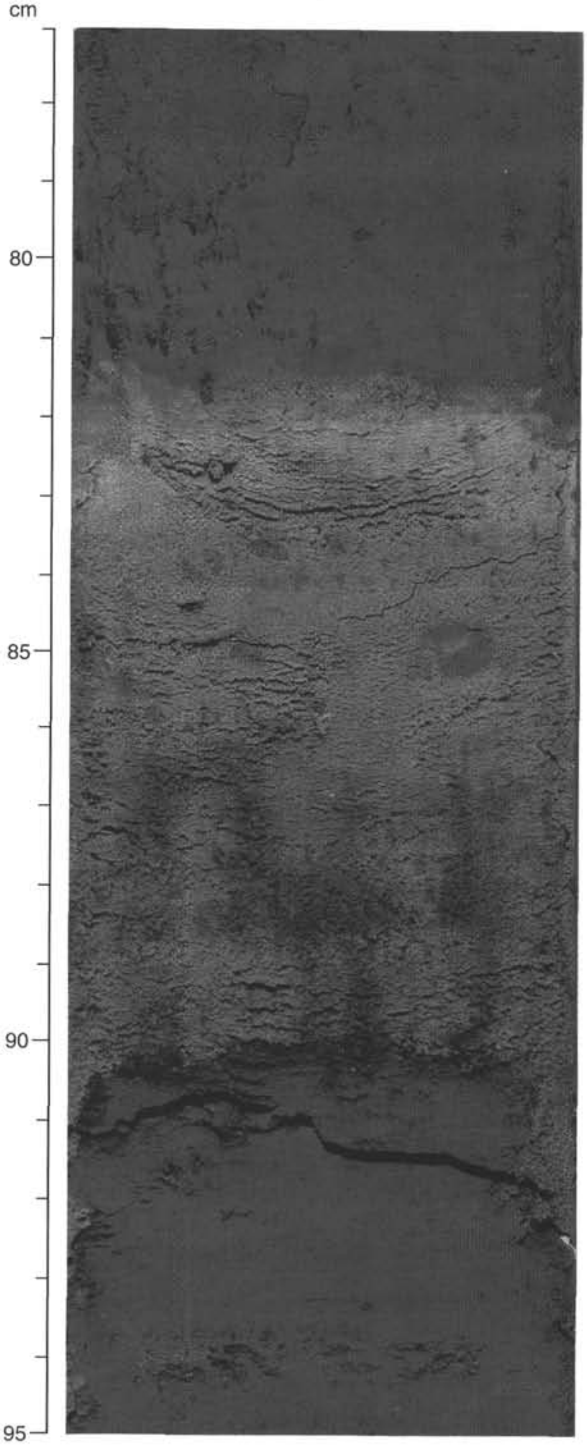

Figure 8. Photograph of an 8-cm colorless volcanic ash layer found in Section 162-983B-17H-6, 77–95 cm.

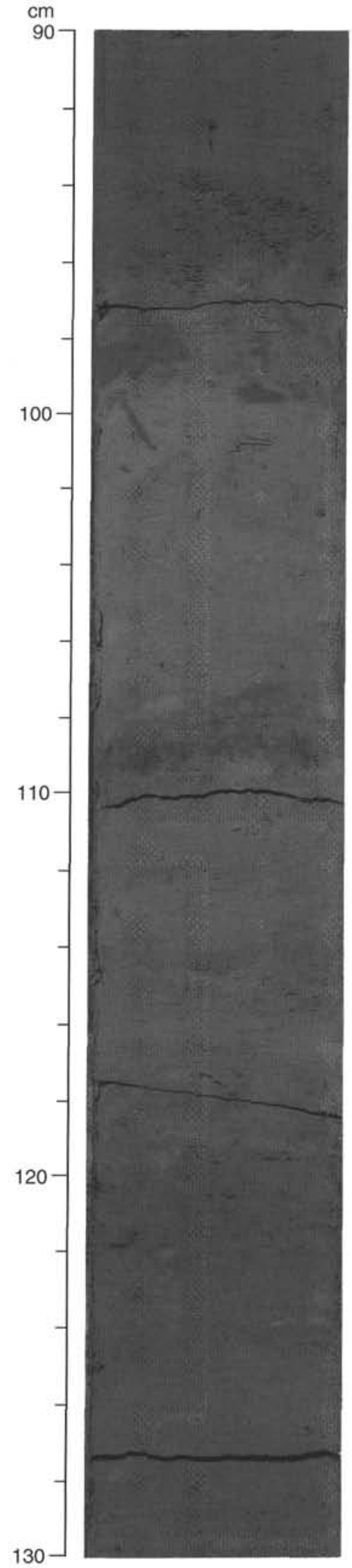

Figure 9. Photograph showing a typical bioturbated color contact in Site 983 sediments (Section 162-983C-11H-5, 90–130 cm).

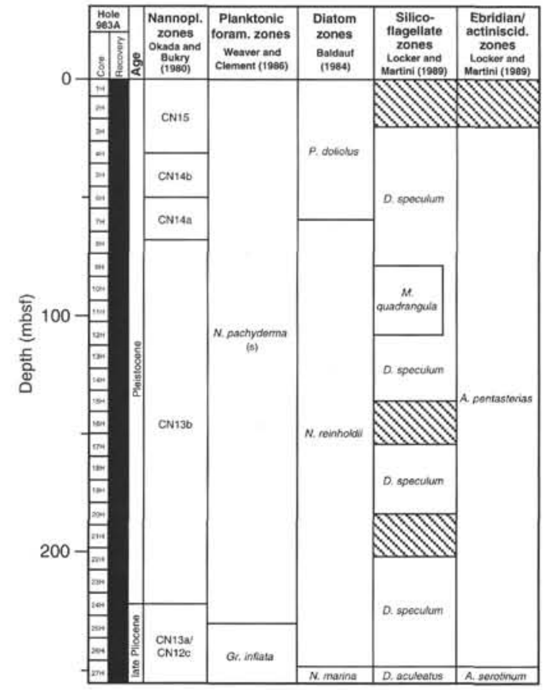

Figure 10. Biostratigraphic summary, Site 983. Hatched intervals indicate absence of fossils. The location of the Pliocene/Pleistocene boundary is based on nannofossil data.

scale. To facilitate comparison between sites, sedimentation rates were estimated from age vs. depth plots by drawing straight-line segments (uniform sedimentation rate) between selected datums.

Sedimentation rates were calculated for both the meters below seafloor (mbsf) depth scale and the meters composite depth (mcd) depth scale. Figure 13 presents sedimentation rates as a function of age and composite depth. Sedimentation rates are calculated based on an integrated magnetobiostratigraphy (Table 9; Fig. 14), and confirm the expected high sedimentation rates for this site. Magnetic polarity age control points included are the Brunhes/Matuyama Chron boundary and the Jaramillo and Olduvai Subchrons. Calcareous nannofossil datums are the FO of *Emilianii huxleyi* at 0.26 Ma, the LO of *Pseudoemilianii lacunosa* at 0.46 Ma, and the LO of *Gephyrocapsa* spp. A/B at 1.23 Ma. These datums are considered synchronous from tropical through temperate zones (see "Biostratigraphy" section, "Explanatory Notes" chapter, this volume).

ORGANIC GEOCHEMISTRY

The shipboard organic geochemistry program at Site 983 consisted of analyses of volatile hydrocarbons, determinations of inorganic carbon, total nitrogen, total carbon, and total sulfur, and pyrolysis measurements (for methods, see "Explanatory Notes" chapter, this volume).

Volatile Hydrocarbon

As part of the shipboard safety and pollution monitoring program, concentrations of methane (C_1), ethane (C_2), and propane (C_3) gases were measured every core using standard ODP headspace-sampling technique. One sample was taken from each core immediately after its arriving on deck and was measured using a Hewlett Packard 5890 Series II gas chromatograph. The results are presented in Table 10 and displayed in Figure 15. Twenty-seven sediment samples were collected between 4.5 and 250.9 mbsf in Hole 983A. Methane concentration in sediments are very low above 120 mbsf (from Sample 162-983A-1H-4, 0–5 cm, to 13H-5, 0–5 cm). Below 120 mbsf, CH_4 concentration shows a distinct downhole increase (Fig. 15). At 241.4 mbsf (Sample 162-983A-26H-5, 0–5 cm), methane concentration reaches a maximum of 8522 ppm (Fig. 15; Table 10). Ethane and propane occur in detectable amounts below 165.4 mbsf (Fig. 15; Table 10).

In general, the C_1/C_2 (methane/ethane) ratios consistently decrease with burial depth due to the increasing influence of early diagenetic generation of hydrocarbons. At Site 983, however, no

Table 6. Depth range of biostratigraphic datums, Site 983.

Datum	Age (Ma)	Core, section, interval (cm)	Depth (mbsf)	Depth (mcd)
		162-983A-		
FO *E. huxleyi* (N)	0.26	3H-CC, 26–29 4H-1, 20–21	26.86 26.60	29.52 30.56
LO *R. curvirostris* (D)	0.30	3H-CC, 26–29 4H-CC, 13–18	26.86 36.32	29.52 40.28
LO *P. lacunosa* (N)	0.46	5H-6, 22–23 5H-CC, 19–24	43.62 45.92	49.43 51.73
LO *N. reinholdii* (D)	0.65	6H-CC, 14–19 7H-CC, 21–24	55.33 64.82	61.29 72.12
FO *Gephyrocapsa* spp. C/D (N)	0.78	8H-3, 10–11 8H-4, 10–11	67.50 69.00	75.37 76.87
LO *M. quadrangula* (S)	0.83	8H-CC, 21–26 9H-CC, 23–28	74.28 83.81	82.15 92.66
LO *H. sellii* (N)	1.22	14H-CC, 21–26 15H-CC, 24–26	131.30 140.94	143.61 153.75
LO *Gephyrocapsa* spp. A/B (N)	1.23	16H-2, 20–21 16H-3, 20–21	142.10 143.60	156.00 157.50
FO *R. curvirostris* (D)	1.58	19H-CC, 23–25 20H-CC, 20–22	178.83 188.28	195.48 205.71
LO *C. macintyrei* (N)	1.59	22H-CC, 24–26 23H-1, 20–21	207.30 207.10	226.34 227.32
FO *Gephyrocapsa* A/B (N)	1.70	23H-7, 20–21 23H-CC, 18–20	216.10 216.68	236.32 236.90
S, acme *N. pachyderma* s. (F)	1.80	25H-2, 20–22 25H-4, 20–22	227.60 230.60	250.41 253.41
FO *P. doliolus* (D)	1.89	26H-CC, 0–3 27H-CC, 24–27	244.99 254.78	269.03 279.47
LO *A. serotinum* (E)	2.00	26H-CC, 0–3 27H-CC, 24–27	244.99 254.78	269.03 279.47

Notes: FO = first occurrence; LO = last occurrence; S = start. In parentheses: N = calcareous nannofossil, D = diatom, S = silicoflagellate, F = planktonic foraminifer, and E = ebridian.

Table 7. Summary of pass-through cryogenic magnetometer measurements at Site 983.

Measurement	Core sections
	162-983A-
25 mT	1H-1 through 27H-6
30 mT	14H-4, 15H-4, 17H-7
	162-982B-
25 mT	1H-1 through 27H-7
30 mT	20H-1, 20H-2, 21H-6, 22H-1, 23H-6
	162-982C-
25 mT	1H-2 through 28H-7
30 mT	13H-4, 15H-6, 16H-1, 28H-3, 28H-4

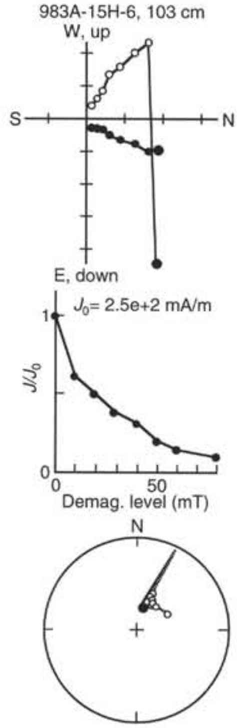

Figure 11. Stepwise AF demagnetization of a sample from Hole 983A. Top: orthogonal projection of end points of the magnetization vector. Open and solid symbols represent projection on the vertical and horizontal planes, respectively. Middle: change in magnetization intensity during AF demagnetization. Bottom: equal area projection of magnetization vector during demagnetization.

significant amounts of higher hydrocarbons (such as ethane or propane) were detected, the high C_1/C_2 ratios suggest a biogenic origin of the methane. The methane at Site 983 was most likely derived from in situ bacterial methanogenesis resulting from decomposition of organic matter in the sediments. The pore-water sulfate concentration is depleted at a depth of about 120 mbsf, where methane starts to increase rapidly (see "Inorganic Geochemistry" section, this chapter).

Carbon, Nitrogen, and Sulfur Concentration

Determinations of inorganic carbon, carbonate, total carbon, total nitrogen, and total sulfur in Hole 983A are summarized in Table 11. Calcium carbonate content in the sediment sequence of Hole 983A fluctuated between 0.7% and 43.3%, with an average value of 16.8% (Fig. 15; Table 11), and shows a gradual decrease with increasing depth. The concentration of carbonate in sediment is primarily controlled by the flux of biogenic carbonate and supply of terrigenous material. As at Sites 980, 981, and 982, the carbonate cycles of Hole 983A certainly reflect glacial/interglacial fluctuations.

Total organic carbon (TOC) contents vary between 0.04% and 0.48%, with an average value of 0.18% (Fig. 15; Table 11). A maximum TOC value of 0.48% occurs in the upper part of the sedimentary record of Hole 983A (Sample 162-983A-5H-2, 43–44 cm; 37.84 mbsf). Total nitrogen contents are generally very low (Fig. 15; Table 11; 0.04%–0.08%). Total sulfur values vary between 0% and 0.59%, with an average value of 0.15% (Fig. 15; Table 11).

Composition of Organic Matter

Due to the organic carbon-poor nature of the sediments, pyrolysis analyses were not made. C/N ratios varied between 0.9 and 9.9 (Fig. 15; Table 11), indicating a predominance of marine organic material (Fig. 16). Further qualitative and quantitative organic geochemical data are required before a detailed paleoceanographic interpretation of the organic carbon data can be made.

INORGANIC GEOCHEMISTRY

Pore-water profiles from Site 983 are typical of sediments in which sulfate reduction and methanogenesis are occurring. Sulfate concentrations decrease from seawater values at the top of the core to zero at about 100 mbsf (Fig. 17A; Table 12). Below 120 mbsf, methane begins to increase from 0 ppm, reaching a maximum of 9000 ppm near the base of the core (Fig. 17B). Methanogenesis is an important process in sediments where sulfate reduction has depleted available sulfate. In this process, organic matter is degraded and carbon dioxide, methane, ammonium, and phosphate are produced with the following Redfield stoichiometry:

$$(CH_2O)_{106}(NH_3)_{16}(H_3PO_4) = 53CO_2 + 53CH_4 + 16NH_3 + H_3PO_4 \quad (1)$$

The boundary between sulfate reduction and methanogenesis is very sharp at Site 983 at 120 mbsf, presumably because utilization of methane by sulfate-reducing bacteria prevents significant diffusive penetration of methane into the sulfate reduction zone above (Gieskes, 1983). The sharp sulfate/methane boundary at 120 mbsf also corresponds with a lithologic subboundary (see "Lithostratigraphy" section, this chapter) and with a seismic reflector (see "Seismic Stratigraphy" section, this chapter).

Ammonia progressively increases with depth due to production by both sulfate reduction and methanogenesis (Fig. 17C; Table 12; Equation 1). Alkalinity increases with depth from 4.5 mM to a maximum of about 13 mM between 80 and 140 mbsf, reflecting bicarbonate production from sulfate reduction (Fig. 17D; Table 12). Below ~130 mbsf, in the zone of methanogenesis, alkalinity decreases, indicating either diminished production or a removal mechanism not related to calcite precipitation, as calcium values increase during this interval (Fig. 17H). Salinity decreases sharply from 34 to 32 in the zone of sulfate reduction, reflecting the removal of dissolved sulfate from pore waters (Fig. 17E; Table 12). Phosphate concentrations generally increase in the top of the core, reaching a maximum at about 80 mbsf, and then decrease toward the bottom of the core, indicating removal of phosphate at depth by mineral precipitation (e.g., francolite).

Magnesium concentrations are near seawater values at the top and decrease linearly downcore (Fig. 17G; Table 12), reflecting (1) uptake by clay mineral formation during in situ alteration of volcanic material in the sediments and (2) chemical interaction with basaltic basement below. Calcium decreases in the upper 80 mbsf from 9.7 mM at the top to a minimum of 3 mM at 80 mbsf, and then increases toward the bottom of the section (Fig. 17H; Table 12). The Ca:Mg relationship is typical of interstitial waters in which both sulfate reduction and alteration of volcanic material are important processes (Fig. 17I). In the upper 80 m, calcium and magnesium show a positive relationship because calcium is decreasing due to precipitation of calcite in the zone of sulfate reduction. Below this level, calcium and magnesium display the typical negative relationship expected from alteration of basaltic material in the oceanic basement and/or dispersed in sediments.

Chloride concentrations increase with depth from near seawater values (~560 mM) to a maximum of 576 mM at 250 mbsf (Fig. 17J; Table 12). Similarly, sodium values also generally increase downcore from near seawater values at the surface (481 mM) to a maximum of 517 mM at the base of the core (Fig. 17K; Table 12). The Na:Cl relationship is linear with a slope of approximately 2:1 (Fig. 17L). The increase in chloride and part of the increase in sodium may result from hydration of clay minerals during in situ alteration of volcanic material (Shipboard Scientific Party, 1995). This process re-

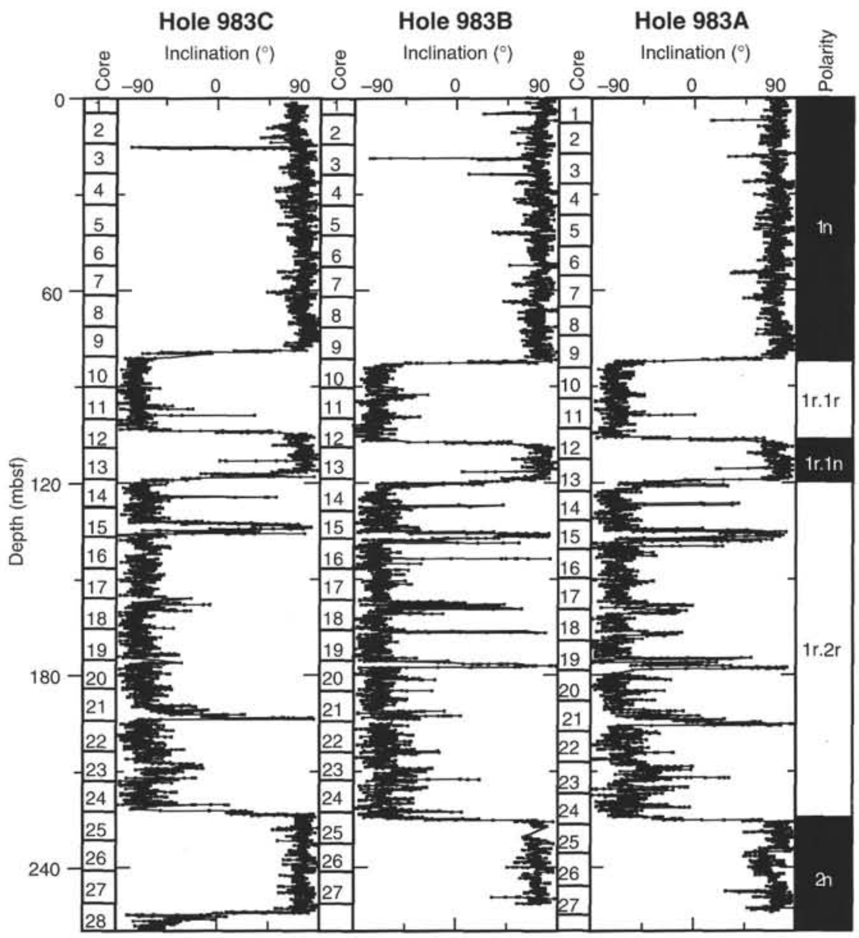

Figure 12. Inclination of the magnetization vector vs. depth (mbsf) for Site 983, after AF demagnetization at peak fields of 25 mT.

Table 8. Preliminary positions of polarity chron boundaries at Site 983.

Core, section, interval (cm)	Depth (mbsf)	Interpreted boundary	Age (Ma)	Comments
162-983A-				
9H-6, 45	81.85	Brunhes/Matuyama	0.78	
12H-3, 90	106.30	Jaramillo (top)	0.99	
13H-6, 0	119.40	Jaramillo (bottom)	1.07	Section break
15H-3, 50	134.40	Cobb Mountain (?)	1.21	
24H-7, 0	225.40	Olduvai (top)	1.77	Section break
162-983B-				
10H-2, 50	82.70	Brunhes/Matuyama	0.78	
12H-6, 40	107.60	Jaramillo (top)	0.99	
14H-2, 30	120.50	Jaramillo (bottom)	1.07	
15H-5, 125	135.35	Cobb Mountain (?)	1.21	
25H-2, 60	225.30	Olduvai (top)	1.77	
162-983C-				
9H-6, 120	79.10	Brunhes/Matuyama	0.78	
12H-4, 50	103.90	Jaramillo (top)	0.99	
14H-1, 0	117.90	Jaramillo (bottom)	1.07	Core break
15H-4, 75	132.65	Cobb Mountain (?)	1.21	
25H-1, 30	222.70	Olduvai (top)	1.77	
28H-3, 75	254.65	Olduvai (bottom)	1.95	

moves water, enriching the remaining pore waters in dissolved constituents. Hydration of clays should enrich both chloride and sodium equally, but the observed 2:1 relationship requires an additional source of dissolved sodium to the pore waters.

Potassium concentrations decrease in the upper 100 m, reflecting uptake into clay minerals, and then values remain relatively constant to the base of the hole (Fig. 17M; Table 12). Lithium concentrations average about 25 μM in the upper 150 m of Site 983 and then increase toward the base of the hole (Fig. 17N; Table 12). This increase probably reflects a diffusion gradient, with oceanic crust below providing a source of lithium to pore waters.

Dissolved silica increases from surface values of 430 μM to a maximum of 945 μM at 165 mbsf, and then values decrease toward the base of the core (Fig. 17O; Table 12). The increasing silica values reflect dissolution of siliceous microfossils and/or alteration of volcanic material. The profile of strontium is similar to that of calcium, showing a modest decrease in the upper 80 mbsf and then increasing steadily toward the base of the core (Fig. 17P; Table 12). The correlation of strontium with calcite is what would be expected from biogenic calcite dissolution and subsequent recrystallization.

PHYSICAL PROPERTIES

Shipboard measurements of sediment physical properties at Site 983 included nondestructive near-continuous measurements of bulk density, bulk magnetic susceptibility, compressional wave (*P*-wave) velocity, and natural gamma radiation on whole-round core sections of the three holes using the multisensor track. Velocities were also measured on split-core sections from Hole 983A, either parallel or perpendicular to the length of the core sections. Measurements were made at an average of six per core. The velocities were measured along core sections above 69.6 mbsf (Table 13). Below this depth the sediment became too consolidated to insert the DSV transducers, and sonic measurements were performed perpendicular to the core axis using the Hamilton Frame velocimeter. Undrained shear strength measurements were made using a motorized vane (Table 14). At approximately 70 mbsf (corresponding to a shear strength of approximately 50 kPa), the vane started to produce cracks in the sediments. A pocket penetrometer was therefore used as an additional tool below this level.

Index properties were measured and calculated according to Method C at a rate of one per section (Table 15). The gravimetric wet bulk density data are generally higher than the GRAPE values (Fig. 18). The difference is approximately 0.1 g/cm^3 in the upper part of the hole but increases to approximately 0.2 g/cm^3 below 210 mbsf. Potential causes for this difference are discussed in "Explanatory Notes" (this volume).

Geotechnical Stratigraphy

One geotechnical unit (G1) has been defined at Site 983, and the physical properties show a gradual downhole effect of increased overburden. The unit consists of two subunits G1A and G1B, primarily defined by the downhole change in velocity. Subunit G1A occupies the uppermost 60 m in Hole 983A, and is characterized by a downhole increase in wet bulk density (from 1.3 to approximately 1.5 g/cm^3), decreasing porosity (from 80% to 70%), fairly low (around 1500 m/s) velocities, and low (about 18 kPa) shear strength values (Fig. 18).

In geotechnical Subunit G1B, the wet bulk density values are quite constant down to 95 mbsf, and increase between 95 and ~155 mbsf (Fig. 18; Table 13). The rest of the hole is characterized by values around 1.6 g/cm^3. The porosity drops from values of 71%–74% to approximately 65%–68% at the bottom of Hole 983A. This trend is inverse to the wet bulk density record, with two intervals of constant values separated by an interval characterized by slightly decreasing values (Fig. 18; Table 13).

There is a good agreement between the two velocity records from the PWL and the split-core measurements, both of which show a gradual increase in velocity downhole due to the effect of increased overburden (Fig. 18). The velocity increases downhole from approximately 1500 m/s near the upper boundary of Subunit G1B to 1530–1550 m/s at the bottom of Hole 983A.

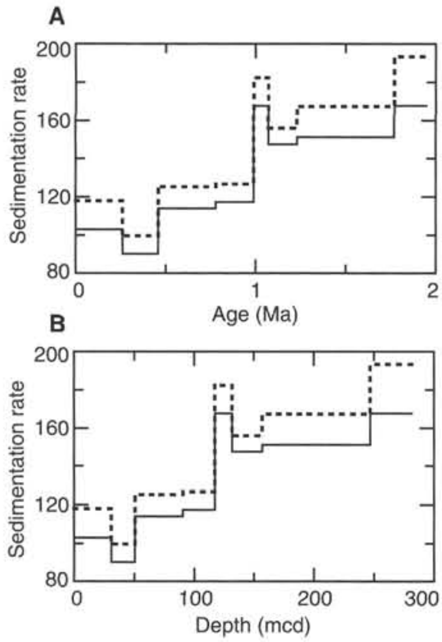

Figure 13. Site 983 sedimentation rates vs. age (**A**) and vs. composite depth (**B**). Solid lines indicate rates in mbsf/m.y.; dashed lines indicate rates in mcd/m.y.

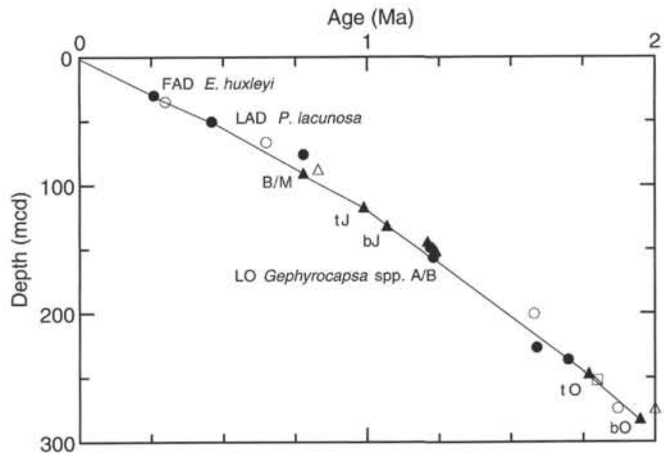

Figure 14. Site 983 age vs. depth (mcd) curve based on integrated magnetostratigraphic and biostratigraphic datums. Solid circles = nannofossils; open circles = diatoms; open squares = foraminifers; open triangles = siliceous flagellates; solid triangles = magnetostratigraphic datums. B/M = Brunhes/Matuyama Chron boundary; tJ and bJ = Jaramillo Subchron (top and bottom); tO and bO = Olduvai Subchron (top and bottom).

Table 9. Age control points, Site 983.

Event	Age (Ma)	983A (mbsf)	983A (mcd)	983B (mbsf)	983B (mcd)	983C (mbsf)	983C (mcd)	Avg. depth (mbsf)	Avg. depth (mcd)	Rate (mbsf/m.y.)	Rate (mcd/m.y.)
Core top	0.00	0.00	0.00	0.00	0.00	0.00	0.02	0.00	0.00		
										102.80	118.04
FO *E. huxleyi* (N)	0.26	26.73	30.69					26.73	30.69		
										90.20	99.45
LO *P. lacunosa* (N)	0.46	44.77	50.58					44.77	50.58		
										113.91	125.25
Brunhes/Matuyama	0.78	81.85	90.70	82.70	90.76	79.10	90.52	81.22	90.66		
										117.37	126.57
Jaramillo top	0.99	106.30	117.12	107.60	117.37	103.69	117.23	105.86	117.24		
										167.54	182.42
Jaramillo bottom	1.07	119.40	131.01	120.50	132.16	117.90	132.33	119.27	131.83		
										147.40	155.73
LO *Gephyrocapsa* spp. A/B (N)	1.23	142.85	156.75					142.85	156.75		
										151.14	167.11
Olduvai top	1.77	225.40	247.36	225.30	247.03	222.70	246.58	224.47	246.99		
										167.69	193.39
Olduvai bottom	1.95					254.65	281.80	254.65	281.80		

Note: Ages are from Berggren et al. (1995). N = calcareous nannofossil.

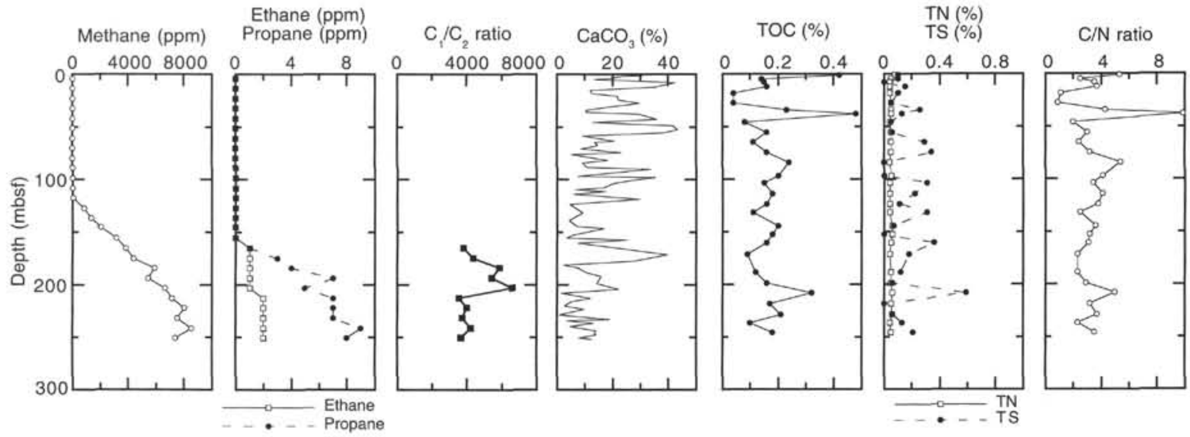

Figure 15. Methane, ethane, and propane concentrations, methane/ethane (C_1/C_2) ratio, calcium carbonate ($CaCO_3$), total organic carbon (TOC), total nitrogen (TN), and total sulfur (TS) contents, and TOC/TN (C/N) ratio in Hole 983A.

Table 10. Results of headspace gas analysis of Hole 983A.

Core, section, interval (cm)	Depth (mbsf)	C_1 (ppm)	C_2 (ppm)	C_3 (ppm)	C_1/C_2	C_1/C_3
162-983A-						
1H-4, 0–5	4.53	2				
2H-5, 0–5	13.43	3				
3H-5, 0–5	22.93	4				
4H-5, 0–5	32.43	5				
5H-5, 0–5	41.93	8				
6H-5, 0–5	51.43	8				
7H-5, 0–5	60.93	8				
8H-5, 0–5	70.43	5				
9H-5, 0–5	79.93	6				
10H-5, 0–5	89.43	6				
11H-5, 0–5	98.93	6				
12H-5, 0–5	108.43	5				
13H-5, 0–5	117.93	32				
14H-5, 0–5	127.43	838				
15H-5, 0–5	136.93	1351				
16H-4, 0–5	144.93	2011				
17H-5, 0–5	155.93	3159				
18H-5, 0–5	165.43	3827	1	1	3827	3827
19H-5, 0–5	174.93	4392	1	3	4392	1464
20H-5, 0–5	184.43	5895	1	4	5895	1474
21H-5, 0–5	193.93	5463	1	7	5463	780
22H-5, 0–5	203.43	6661	1	5	6661	1332
23H-5, 0–5	212.93	7171	2	7	3586	1024
24H-5, 0–5	222.43	8024	2	7	4012	1146
25H-5, 0–5	231.93	7529	2	7	3765	1076
26H-5, 0–5	241.43	8522	2	9	4261	947
27H-5, 0–5	250.93	7398	2	8	3699	925

Notes: C_1 = methane, C_2 = ethane, C_3 = propane, C_1/C_2 = methane/ethane ratio, C_1/C_3 = methane/propane ratio.

The undrained shear strength record shows a downhole trend caused by a gradually increased downhole overburden (Fig. 18; Table 14). The values near the upper boundary of Subunit G1B are close to 30 kPa, and increase downhole to approximately 100 kPa (vane) and 177 kPa (pocket penetrometer) at the bottom of the hole.

The magnetic susceptibility record shows a large number of peaks (Fig. 18) throughout Hole 983A, suggesting that during the last 2 m.y. (see "Biostratigraphy" and "Paleomagnetism" sections, this chapter) accumulation of terrigenous material at the site has followed a cyclic pattern. Increases in magnetic susceptibility appear to correlate with peaks in shear strength below ~170 mbsf, suggesting that shear strength increases in zones that contain relatively more continental-derived material with high susceptibilities.

The natural gamma radiation record from Hole 983A also reveals a cyclic pattern consisting of high and low counts (Fig. 18). The peaks most likely reflect zones enriched in clay minerals. The frequency pattern with which the peaks appear is similar to that of the magnetic susceptibility, but the cycles are not in phase. Thus, fluctuations in clay/carbonate accumulation are not necessarily driven by the same factors that control the frequencies of terrigenous material deposition at the site.

Correlation with Lithostratigraphy and Seismic Stratigraphy

Hole 983A penetrates three seismic reflectors at 60, 121, and 163 mbsf, respectively (see "Seismic Stratigraphy" section, this chapter), and recovered one lithostratigraphic unit which has been divided into three subunits (see "Lithostratigraphy" section, this chapter). Reflectors R1 and R2 correspond to lithostratigraphic boundaries, but Reflector R3 does not seem to correspond to changes in lithology. Reflector R1 is most likely associated with the change in velocity that occurs at approximately 60 mbsf (Fig. 18), which may produce a change in acoustic impedance. Reflectors R2 and R3 are relatively strong, and may be associated with velocity peaks that occur at 121 mbsf and close to 160 mbsf, respectively (Fig. 18).

Physical properties in Hole 983A suggest that the entire drilled section is continuous, without significant stratigraphic breaks. This is in agreement with the biostratigraphic studies (see "Biostratigraphy" section, this chapter). The conformable nature of the sediments is also reflected by the internal seismic reflection pattern of the sedimentary basin at Site 983 (see "Seismic Stratigraphy" section, this chapter). The general picture of the sediments as viewed from their physical properties is in good agreement with their lithology, which is characterized by rapidly accumulated fine-grained terrigenous and biogenic sediments (see "Lithostratigraphy" section, this chapter).

SEISMIC STRATIGRAPHY

The proposed site GARDAR-1 (Site 983) was selected on the basis of the multichannel seismic EW-9302 Line 1b, shot in 1993 (Oppo et al., unpubl. data). To obtain a crossing line and to survey GGC-11, a nearby giant gravity core site off the existing seismic line, a survey was designed to connect the two sites and then duplicate EW-9302 Line 1b. The survey (Fig. 19) was carried out using the 80-in.[3] water gun as source (see "Explanatory Notes" chapter, this volume), as well as the 3.5-kHz and 12-kHz PDR systems. In order to tie the drill site to results from pre-cruise gravity cores, PDR data were considered to be of particular importance. The pre-cruise seismic data showed that the area is characterized by a high basement relief, and it was therefore important to locate the site between basement highs. Furthermore, the survey showed that the sedimentary section in this area is disrupted by small faults associated with the basement highs.

Table 11. Summary of organic geochemical analyses of Hole 983A samples.

Core, section, interval (cm)	Depth (mbsf)	IC (%)	$CaCO_3$ (%)	TC (%)	TOC (%)	TN (%)	TS (%)	C/N
162-983A-								
1H-1, 107–108	1.08	3.68	30.7	4.10	0.42	0.08	0.10	5.3
1H-2, 40–41	1.91	2.86	23.8					
1H-3, 134–135	4.35	2.18	18.2					
1H-4, 33–34	4.84	1.65	13.7	1.79	0.14	0.05	0.10	2.5
2H-1, 62–63	8.03	5.09	42.4	5.24	0.15	0.04	0.00	3.5
2H-4, 63–64	12.54	4.23	35.2	4.39	0.16	0.04	0.15	3.7
2H-6, 59–60	15.50	1.44	12.0					
3H-1, 124–125	18.15	1.49	12.4	1.53	0.04	0.04	0.10	1.1
3H-3, 72–73	20.63	2.61	21.7					
3H-5, 125–126	24.16	2.68	22.3					
4H-1, 81–82	27.22	3.58	29.8	3.62	0.04	0.05	0.05	0.9
4H-4, 92–93	31.83	2.02	16.8					
4H-6, 14–15	34.05	1.25	10.4	1.48	0.23	0.05	0.26	4.3
4H-7, 37–38	35.78	1.29	10.7					
5H-2, 43–44	37.84	3.54	29.5	4.02	0.48	0.05	0.13	9.9
5H-5, 80–81	42.71	4.33	36.1					
6H-1, 70–71	46.11	1.56	13.0	1.64	0.08	0.04	0.05	2.0
6H-3, 27–28	48.68	5.02	41.8					
6H-5, 129–130	52.70	5.20	43.3					
7H-1, 68–69	55.59	4.63	38.6	4.79	0.16	0.05	0.06	3.0
7H-3, 59–60	58.50	1.12	9.3					
7H-6, 79–80	63.20	2.47	20.6					
8H-1, 58–59	64.99	1.63	13.6	1.74	0.11	0.05	0.29	2.4
8H-3, 70–71	68.11	1.76	14.7					
8H-5, 47–48	70.88	1.06	8.8					
9H-1, 73–74	74.64	2.79	23.2	2.95	0.16	0.05	0.34	3.2
9H-2, 89–90	76.30	0.62	5.2					
9H-6, 7–68	82.08	2.19	18.2					
10H-1, 80–81	84.21	1.11	9.2	1.35	0.24	0.04	0.00	5.4
10H-4, 75–76	88.66	1.30	10.8					
10H-5, 83–84	90.24	4.02	33.5					
11H-3, 139–140	97.30	0.89	7.4	1.09	0.20	0.05	0.00	4.1
11H-4, 117–118	98.58	4.22	35.2					
11H-6, 50–51	100.91	3.31	27.6					
12H-1, 135–136	103.76	2.46	20.5	2.61	0.15	0.04	0.31	3.4
12H-4, 101–102	107.92	2.03	16.9					
12H-5, 134–135	109.75	0.81	6.7					
12H-7, 57–58	111.98	2.11	17.6					
13H-2, 99–100	114.40	0.73	6.1	0.91	0.18	0.04	0.22	4.1
13H-5, 99–100	118.90	3.57	29.7					
14H-2, 102–103	123.93	0.55	4.6	0.71	0.16	0.04	0.11	3.8
15H-1, 100–101	131.91	1.10	9.2	1.21	0.11	0.04	0.31	2.5
15H-6, 101–102	139.42	0.52	4.3					
16H-3, 133–134	144.74	0.87	7.2	1.07	0.20	0.06	0.07	3.6
16H-4, 138–139	146.29	2.06	17.2					
16H-5, 98–99	147.39	1.93	16.1					
17H-2, 129–130	152.70	0.76	6.3	0.94	0.18	0.06	0.00	3.2
17H-4, 128–129	155.69	0.43	3.6					
17H-5, 122–123	157.13	3.06	25.5					
18H-1, 135–136	160.76	0.91	7.6	1.07	0.16	0.05	0.36	3.1
18H-4, 128–129	165.19	2.66	22.2					
19H-2, 137–138	171.78	4.78	39.8	4.87	0.09	0.04	0.18	2.3
19H-6, 135–136	177.76	3.33	27.7					
20H-2, 115–116	181.06	3.38	28.2	3.60	0.22	0.05	0.27	4.5
20H-4, 127–128	184.18	0.96	8.0					
20H-4, 135–136	184.26	0.93	7.7					
21H-1, 81–82	188.72	1.28	10.7	1.40	0.12	0.05	0.12	2.3
21H-3, 130–131	192.21	1.91	15.9					
22H-1, 137–138	198.78	1.73	14.4	1.89	0.16	0.05	0.06	2.9
22H-5, 130–131	204.71	2.66	22.2					
23H-1, 139–140	208.30	0.20	1.7	0.52	0.32	0.06	0.59	5.0
23H-4, 139–140	212.80	1.44	12.0					
23H-6, 134–135	215.75	0.62	5.2					
24H-2, 78–79	218.69	0.44	3.7	0.61	0.17	0.05	0.00	3.2
24H-3, 97–98	220.38	0.34	2.8					
24H-5, 117–118	223.58	1.16	9.7					
25H-2, 119–120	228.60	0.09	0.7	0.30	0.21	0.06	0.06	3.7
25H-5, 121–122	233.12	2.27	18.9					
25H-6, 112–113	234.53	0.43	3.6					
26H-1, 131–132	236.72	1.56	13.0	1.66	0.10	0.04	0.13	2.3
26H-3, 130–131	239.71	0.56	4.7					
26H-6, 122–123	244.13	1.70	14.2					
27H-1, 130–131	246.21	1.65	13.7	1.83	0.18	0.05	0.21	3.5
27H-2, 130–131	247.71	1.68	14.0					
27H-4, 116–117	250.57	0.95	7.9					
27H-5, 123–124	252.14	1.49	12.4					

Notes: IC = inorganic carbon, $CaCO_3$ = calcium carbonate, TC = total carbon, TOC = total organic carbon, TN = total nitrogen, TS = total sulfur, and C/N = total organic carbon/total nitrogen ratios.

The site survey revealed that the originally proposed site was near optimal, both with respect to distance from any obvious faults, and the thickness and continuous character of the sedimentary section. The position chosen for the site was therefore within a 100-m radius of the original, and corresponds to shotpoint 669 of Line S3 (Fig. 20).

Description of Seismic Stratigraphic Units

Seven seismic units (GA-I to GA-VII; Fig. 20B) were defined from the site survey data, but only the upper four were penetrated during drilling at Site 983. The sedimentary section as a whole is acoustically well stratified, although variable between units. Lateral changes in sediment thickness are common and seem to be controlled by basement relief as well as by depositional and erosional processes.

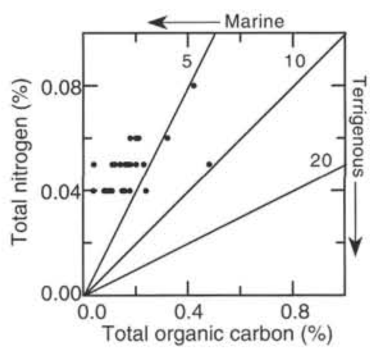

Figure 16. Total organic carbon vs. total nitrogen in Hole 983A. Lines show C/N ratios of 5, 10, and 20.

Basement shows high relief, resulting from the formation of half grabens, each bounded by steep normal faults on its eastern side. The sediments fill the basins in between the basement highs, and closely spaced faulting of the sedimentary section is observed primarily over the highs. As at Site 982 (see "Site 982" chapter, this volume), the faults extend to the seafloor, where they produce small depressions. Faulting can readily be observed in the high-resolution 3.5-kHz PDR records (Fig. 21), and the displacement rarely exceeds 7–8 m.

The seismic stratigraphy is based on the identification of six significant seismic reflectors (R1 through R6) between the seafloor and acoustic basement. In addition to marking changes in seismic character, these reflectors also become unconformities when traced laterally away from Site 983. Erosional truncation of underlying strata, as well as onlapping reflectors are observed, with the latter being more prominent towards the margins of each individual basin. With the exception of Reflector R1, the erosion related to each of these unconformities does not appear to be significant as judged from the seismic records alone. At Site 983, all seismic reflectors are conformable, suggesting that no major hiatuses would be found at the site.

Unit GA-I extends from the seafloor at 2.755 seconds two-way traveltime (s TWT) to approximately 2.835 s TWT (Fig. 22). This unit is penetrated by the 3.5-kHz PDR (Fig. 21), and displays a distinct layering of evenly spaced reflectors. The distance between individual reflectors in the PDR records is about 10–12 ms TWT at Site 983. Using an interval velocity of 1.55 km/s, as measured on split cores (see "Physical Properties" section, this chapter) and adjusted for core expansion (see "Explanatory Notes" chapter, this volume), the spacing of reflectors is 8–9 m and the total thickness of Unit GA-I is about 60 m. In the lower resolution seismic section, this unit appears as an almost acoustically transparent layer. Farther east along Line S1, Reflector R1 seems to be a major unconformity in the upper

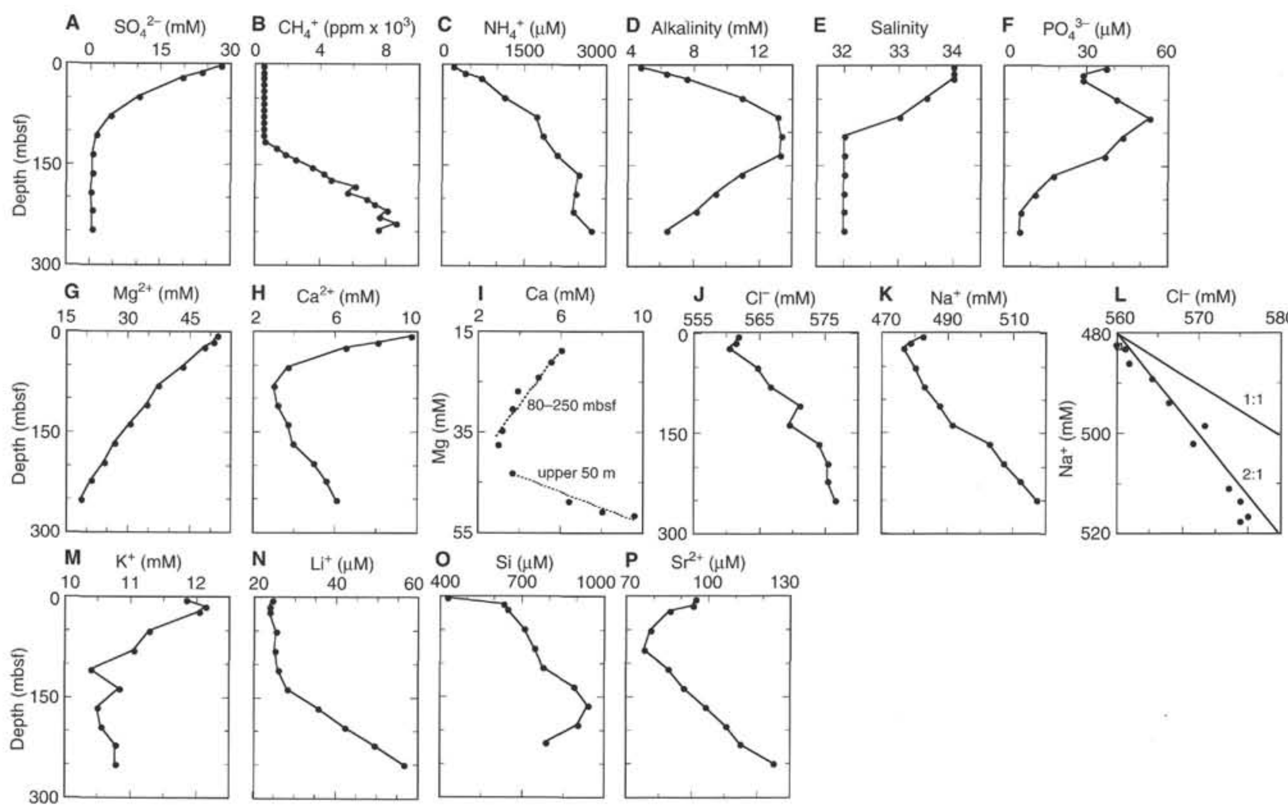

Figure 17. Vertical profiles of interstitial waters and comparisons of interstitial components: sulfate (**A**), headspace methane (**B**), ammonium (**C**), alkalinity (**D**), salinity (**E**), phosphate (**F**), magnesium (**G**), and calcium (**H**), calcium vs. magnesium (**I**), chloride (**J**), sodium (**K**), sodium vs. chloride (**L**), potassium (**M**), lithium (**N**), silica (**O**), and strontium (**P**) in Hole 983A.

Table 12. Composition of interstitial waters in Hole 983A.

Core, section, interval (cm)	Depth (mbsf)	Na (mM)	K (mM)	Li (μM)	Mg (mM)	Ca (mM)	Sr (μM)	Cl (mM)	SO_4 (mM)	NH_4 (μM)	Si (μM)	PO_4 (μM)	pH	Alkalinity (mM)	Salinity
162-983A-															
1H-3, 145–150	4.45	485	11.8	19.0	51.9	9.7	94	561	27.6	217	429	37.1	7.61	4.575	34.0
2H-4, 145–150	13.35	482	12.1	18.4	51.1	8.0	93	561	23.5	430	637	28.6	7.54	6.164	34.0
3H-4, 145–150	22.85	482	12.0	18.3	49.0	6.4	86	560	19.3	717	646	28.9	7.62	7.483	34.0
6H-4, 145–150	51.35	488	11.3	19.9	43.5	3.6	81	564	10.2	1144	709	41.0	7.63	10.851	33.5
9H-4, 145–150	79.85	493	11.0	19.1	37.7	2.9	74	566	4.1	1728	745	53.4	7.88	13.057	33.0
12H-4, 145–150	108.35	498	10.4	20.7	34.8	3.1	81	570	1.0	1864	780	43.4	7.75	13.291	32.0
15H-4, 145–150	136.85	501	10.8	22.7	30.6	3.6	86	569	0.2	2111	893	36.8	7.83	13.186	32.0
18H-4, 145–150	165.35	510	10.5	30.4	26.9	3.9	93	573	0.3	2511	945	17.8	7.83	10.839	32.0
21H-4, 145–150	193.85	513	10.5	36.9	24.3	4.9	99	575	0.0	2478	906	11.1	7.72	9.247	32.0
24H-4, 145–150	222.35	517	10.7	44.4	21.1	5.5	103	575	0.1	2420	792	6.0	7.80	8.067	32.0
27H-4, 145–150	250.85	516	10.7	51.4	18.6	6.0	113	576	0.2	2747		5.4	8.01	6.267	32.0

Table 13. Compressional-wave velocity measurements from Hole 983A.

Core, section, interval (cm)	Depth (mbsf)	Velocity (m/s)	Temperature (°C)	Direction
162-983A-				
1H-1, 36	0.36	1512	20.7	z
1H-1, 108	1.08	1511	19.5	z
1H-2, 41	1.91	1507	18.9	z
1H-2, 121	2.71	1503	19.9	z
1H-3, 66	3.66	1501	20.3	z
1H-4, 87	5.37	1496	20.2	z
1H-5, 53	6.53	1499	20.2	z
2H-1, 63	8.03	1499	20.0	z
2H-2, 89	9.79	1492	19.4	z

Note: For explanation of measurement directions, see "Explanatory Notes" chapter (this volume).

Only part of this table is reproduced here. The entire table appears on the CD-ROM (back pocket).

Table 14. Undrained shear strength measurements from Hole 983A.

Core, section, interval (cm)	Depth (mbsf)	Undrained shear strength (kPa)	Spring no.	Penetrometer (kPa)
162-983A-				
1H-1, 42	0.42	8.8	1	
1H-2, 41	1.91	8.7	1	
1H-2, 120	2.70	24.8	1	
1H-3, 65	3.65	7.4	1	
1H-4, 87	5.37	12.9	1	
1H-5, 51	6.51	30.6	1	
2H-1, 62	8.02	12.2	1	
2H-2, 88	9.78	20.7	1	
2H-3, 17	10.57	6.3	1	

Only part of this table is reproduced here. The entire table appears on the CD-ROM (back pocket).

Table 15. Index properties of samples from Hole 983A.

Core, section, interval (cm)	Depth (mbsf)	Water content (wet %)	Water content (dry %)	Bulk density Method C (g/cm^3)	Grain density Method C (g/cm^3)	Dry density Method C (g/cm^3)	Porosity Method C (%)	Void ratio Method C
162-983A-								
1H-1, 35–37	0.35	61.1	157.4	1.34	2.63	0.52	80.1	4.03
1H-1, 106–108	1.06	63.4	173.5	1.30	2.44	0.48	80.5	4.12
1H-2, 40–42	1.90	57.2	133.4	1.41	2.86	0.61	78.8	3.72
1H-2, 119–121	2.69	56.0	127.2	1.41	2.69	0.62	76.9	3.34
1H-3, 64–66	3.64	56.5	130.0	1.40	2.71	0.61	77.5	3.44
1H-3, 134–136	4.34	61.0	156.3	1.34	2.61	0.52	79.9	3.98
1H-4, 32–34	4.82	60.6	153.5	1.33	2.49	0.53	78.9	3.73
1H-4, 86–88	5.36	65.2	187.3	1.32	2.93	0.46	84.3	5.35
1H-5, 51–53	6.51	55.5	124.8	1.42	2.74	0.63	77.0	3.34

Only part of this table is reproduced here. The entire table appears on the CD-ROM (back pocket).

part of the sedimentary section, and most of the sequence drilled at Site 983 pinches out against Reflector R1 within a distance of 12 km east of the site.

Unit GA-II, bounded by Reflectors R1 and R2, thins both westward and eastward of Site 983. Its thickness is approximately the same as that of Unit GA-I, extending from 60 to 125 mbsf (Figs. 20, 22) and appears slightly more acoustically stratified than the upper unit.

The next seismic unit, GA-III, differs from the two upper units in having distinct, closely spaced, high-amplitude reflectors, both internally and as its upper and lower boundary Reflectors R2 and R3, respectively. Both reflectors are unconformities, with onlapping overlying reflectors, but none of them appear to be erosional in character. Toward the east, both Reflectors R2 and R3 terminate against R1. The seismic velocities measured for this site show no distinct steps, but rather a small but steady downhole increase. Using an interval velocity of 1.6 km/s, Unit GA-III extends from 125 mbsf to approximately 170 mbsf.

Drilling at Site 983 terminated approximately 85 m into seismic Unit GA-IV (Fig. 22). Using an interval velocity of 1.65 km/s in the upper part, and slightly higher, 1.8 km/s, below, this unit extends from 170 to about 420 mbsf. The lower boundary is uncertain, however, since velocity measurements do not exist for most of the unit. Most of this seismic unit also pinches out against Reflector R1 in the eastern part of the survey area (Fig. 20). Unit GA-IV shows generally low-amplitude stratification, although some variation is observed. Reflections are slightly stronger in the upper part of the unit than in the lower. At mid-depths, 10–20 m below the bottom of Hole 983A, a wide reflector, consisting of a band of individual reflections, is seen. The base of this unit, Reflector R4, shows the same unconformable but nonerosive character as Reflectors R2 and R3, with onlapping strata towards the margins of the sub-basin in which Site 983 is located. A similar reflection configuration is even better developed in the larger sub-basin farther east along Line S2 (Fig. 20).

Unit GA-V is defined between Reflectors R4 and R5, from 3.270 s and 3.485 s TWT below seafloor. It is characterized by high-ampli-

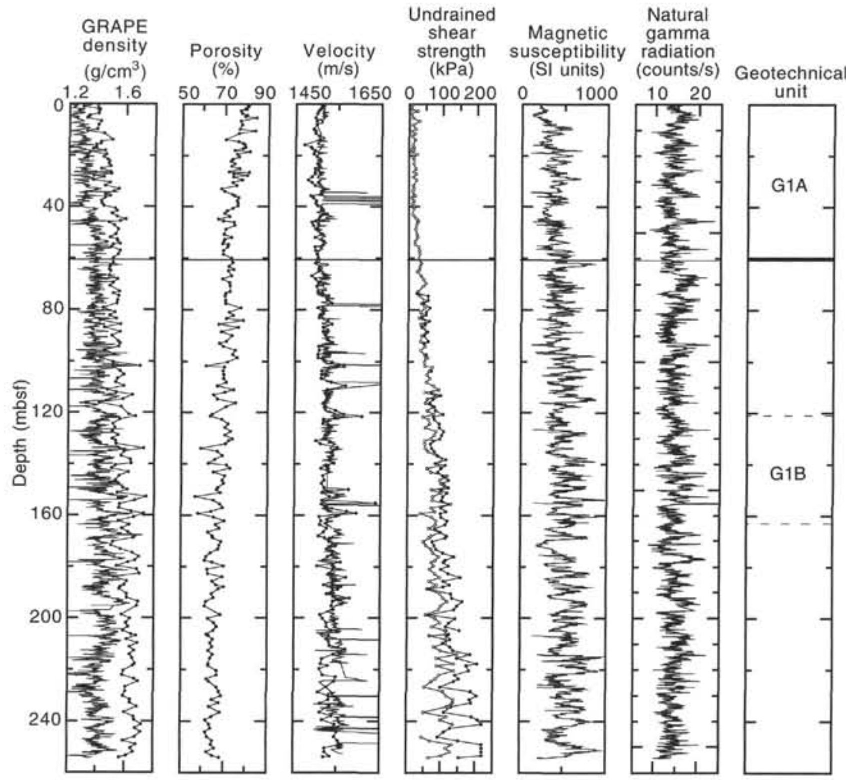

Figure 18. Plots of GRAPE wet bulk density (thin line) and gravimetric bulk density (line with solid circles), porosity, *P*-wave velocity (thin line) and split-core velocity (line with solid circles), undrained shear strength (vane = open circles; pocket penetrometer = solid circles), magnetic susceptibility, natural gamma radiation and geotechnical stratigraphy (with seismic Reflectors R2 and R3 marked by dashed lines) for Hole 983A.

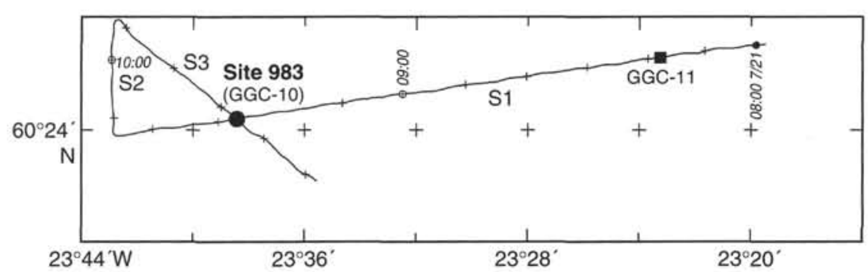

Figure 19. Map showing the site survey at Site 983. GGC-10 and GGC-11 are giant gravity coring stations from pre-cruise site survey.

tude stratification, and the lower strata onlap the basal Reflector R5. Again, as for Unit GA-IV, this is best developed in the eastern subbasin (Fig. 20), but is also clearly observed near Site 983.

The disposition of the two lowermost units, GA-VI and GA-VII, is controlled by the underlying basement topography to a higher degree than that of the overlying units. Unit GA-VI has a band of relatively strong reflections in its upper part, with decreasing amplitudes downsection. Unit GA-VII, on the other hand, is nearly transparent, with the exception of a strong, flat reflector approximately 0.1 s TWT above basement.

Relationship to Core Data

The sediments cored at Site 983 are homogeneous in character and comprise only one lithostratigraphic unit. Subdivision into the three lithostratigraphic Subunits IA, IB, and IC is based on subtle changes in the carbonate vs. terrigenous content and in the spectral reflectivity trend (see "Lithostratigraphy" section, this chapter). The cyclic character of the upper sedimentary section, as observed in the 3.5-kHz PDR records (Fig. 21), is probably caused by these changes, and could therefore be related to lithologic differences between glacial and interglacial periods. The boundary between lithostratigraphic Subunits IA and IB corresponds to seismic Reflector R2, while the lower lithostratigraphic subunit boundary is defined approximately 10 m below Reflector R3 (Fig. 22).

The shipboard measurements of sediment physical properties show steady, normal trends of increasing compaction with depth, and only one geotechnical unit, consisting of two subunits, G1A and G1B, is defined (see "Physical Properties" section, this chapter). The *P*-wave velocity curve shows distinct highs of approximately 50 m/s above the average trend both at 120–125 mbsf and around 160 mbsf. These depths correspond to Reflector R2 and near Reflector R3, respectively. At 160 mbsf, there is also a general increase in the velocity gradient vs. depth. The geochemical characteristics of the sediments also change at 120 mbsf, in association with a pronounced increase in methane concentration (see "Inorganic Geochemistry" and "Organic Geochemistry" sections, this chapter).

Overall, the correlation between seismic unit boundaries and sedimentary changes is good. Reflector R1 is defined because it changes into a main unconformity both westward and eastward of the site. Based on seismic data alone, no significant change in the cored sediments was to be expected at this level. Reflector R2, however, corresponds to noticeable changes in lithology, as well as in physical and geochemical properties.

The seismic data show that the Gardar Drift represents a dynamic depositional environment. About 1 km of sediment fills the basins

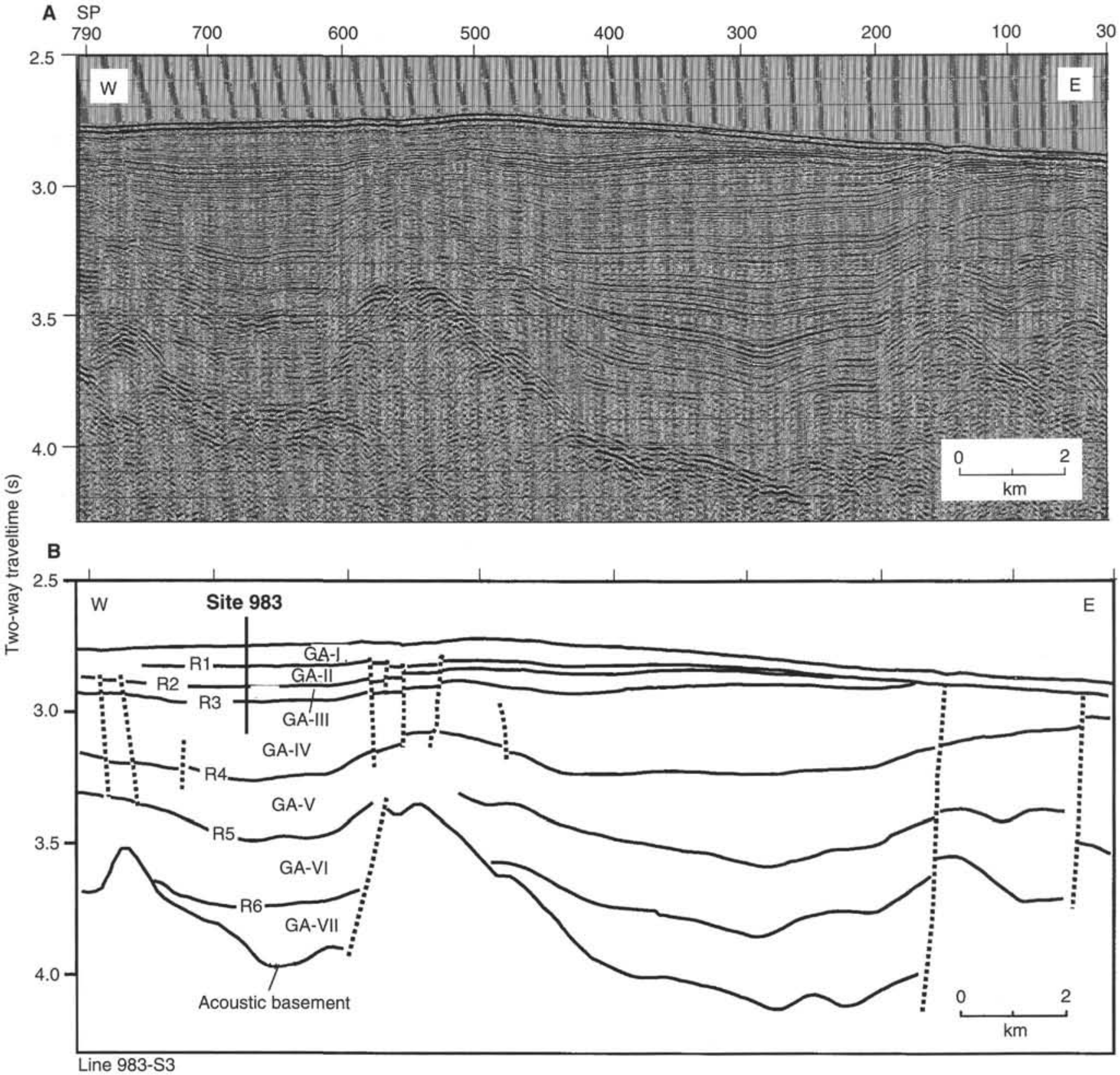

Figure 20. **A.** Seismic Line 983-S1. **B.** Interpretation of Line 983-S3, with seismic units and reflectors shown. The figure shows the entire line. See Figure 19 for location.

formed between basement highs. The thickness of individual stratigraphic units shows large lateral variability, and onlap relationships may indicate near-bottom sediment transport and/or syndepositional tectonic movements. Only the upper seismic unit boundary, Reflector R1, is clearly erosional in character when followed laterally away from the site. At Site 983, all seismic reflectors are conformable, and the seismic stratigraphy supports the results from other shipboard investigations, namely that the drilled sequence represents a continuous sedimentary section.

REFERENCES

Baldauf, J.G., 1984. Cenozoic diatom biostratigraphy and paleoceanography of the Rockall Plateau region, North Atlantic, Deep Sea Drilling Project Leg 81. *In* Roberts, D.G., Schnitker, D., et al., *Init. Repts. DSDP,* 81: Washington (U.S. Govt. Printing Office), 439–478.

Berggren, W.A., Hilgen, F.J., Langereis, C.G., Kent, D.V., Obradovich, J.D., Raffi, I., Raymo, M.E., and Shackleton, N.J., 1995. Late Neogene chronology: new perspectives in high-resolution stratigraphy. *Geol. Soc. Am. Bull.,* 107:1272–1287.

Bond, G., Broecker, W., Johnsen, S., McManus, J., Labeyrie, L., Jouzel, J., and Bonani, G., 1993. Correlations between climate records from the North Atlantic sediments and Greenland ice. *Nature,* 365:143–147.

Bond, G., Heinrich, H., Broecker, W., Labeyrie, L., McManus, J., Andrews, J., Huon, S., Janitschik, R., Clasen, S., Simet, C., Tedesco, K., Klas, M., Bonani, G., and Ivy, S., 1992. Evidence for massive discharge of icebergs into the North Atlantic ocean during the last glacial period. *Nature,* 360:245–249.

Bond, G.C., and Lotti, R., 1995. Iceberg discharges into the North Atlantic on millennial time scales during the last glaciation. *Science,* 276:1005–1010.

Boyle, E.A., and Keigwin, L.D., 1987. North Atlantic thermohaline circulation during the past 20,000 years linked to high-latitude surface temperature. *Nature,* 330:35–40.

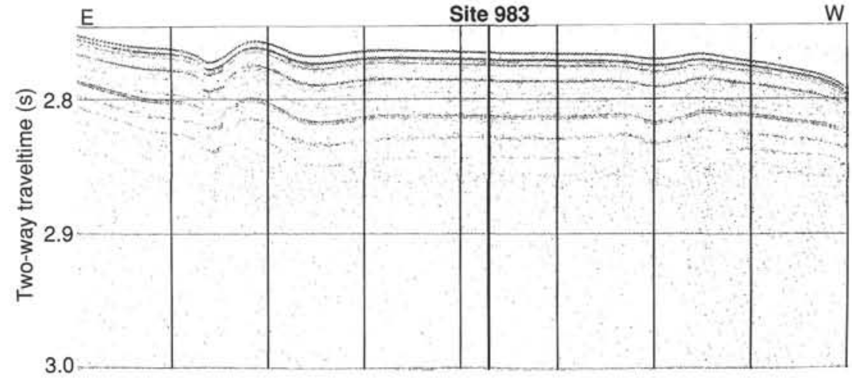

Figure 21. Sample of 3.5-kHz PDR record along Line S1. Note the evenly spaced reflectors.

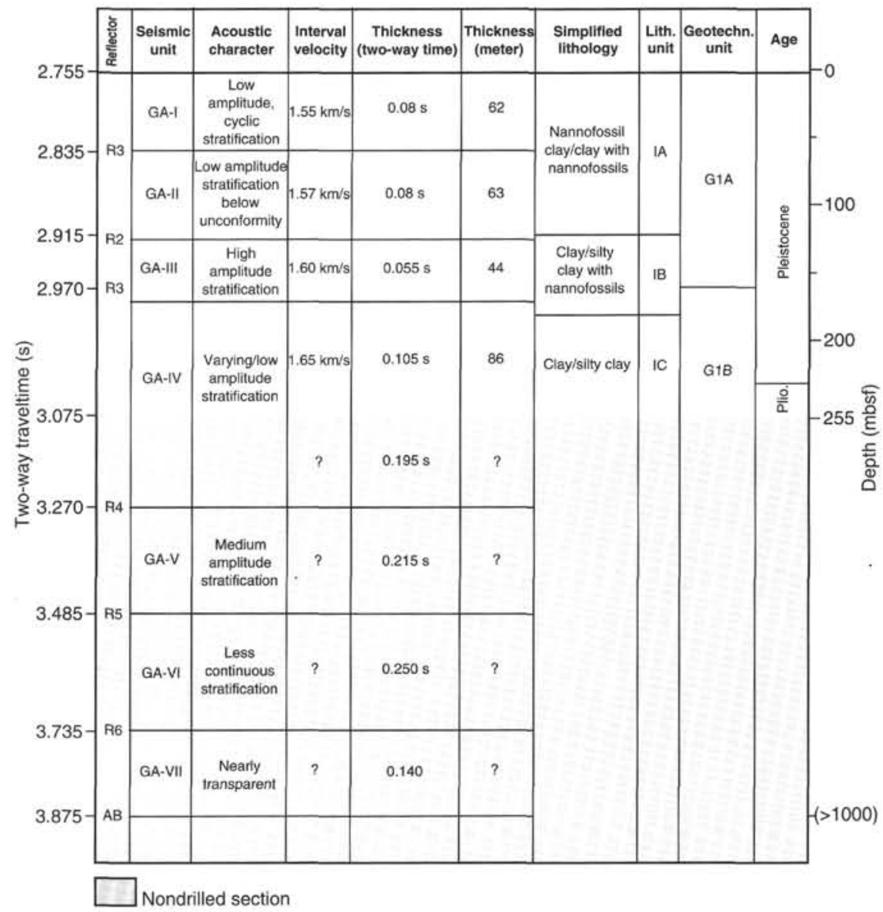

Figure 22. Relationships between seismic stratigraphy, lithostratigraphy, and geotechnical stratigraphy. The depth scale in mbsf is linear within the depths drilled, but note that the figure is not to scale below the drilled depth. AB = acoustic basement.

Broecker, W.S., 1994. Massive iceberg discharges as triggers for global climate change. *Nature,* 372:421–424.

Donnally, D.M., 1989. Calcareous nannofossils of the Norwegian-Greenland Sea: ODP Leg 104. *In* Eldholm, O., Thiede, J., Taylor, E., et al., *Proc. ODP, Sci. Results,* 104: College Station, TX (Ocean Drilling Program), 459–486.

Fronval, T., Jansen, E., Bloemendal, J., and Johnsen, S., 1995. Oceanic evidence for coherent fluctuations in Fennoscandian and Laurentide ice sheets on millennium timescales. *Nature,* 374:443–446.

Gieskes, J.M., 1983. The chemistry of interstitial waters of deep-sea sediments: interpretation of deep-sea drilling data. *In* Riley, J.P., and Chester, R. (Eds.), *Chemical Oceanography* (Vol. 8): London (Academic), 222–269.

Heinrich, H., 1988. Origin and consequences of cyclic ice rafting in the northeast Atlantic Ocean during the past 130,000 years. *Quat. Res.,* 29:142–152.

Locker, S., and Martini, E., 1989. Cenozoic silicoflagellates, ebridians, and actiniscidians from the Vøring Plateau (ODP Leg 104). *In* Eldholm, O., Thiede, J., Taylor, E., et al., *Proc. ODP, Sci. Results,* 104: College Station, TX (Ocean Drilling Program), 543–585.

MacAyeal, D., 1993. Binge/purge oscillations of the Laurentide ice sheet as a cause of the North Atlantic's Heinrich events. *Paleoceanography,* 8:775–795.

McCartney, M.S., 1992. Recirculating components to the deep boundary current of the northern North Atlantic. *Prog. Oceanogr.,* 29:283-383.

McCave, I.N., and Tucholke, B.E., 1986. Deep current-controlled sedimentation in the western North Atlantic. *In* Vogt, P.R., and Tucholke, B.E. (Eds.), *The Western North Atlantic Region.* Geol. Soc. Am., Geol. of North Am. Ser., M:451–468.

Okada, H., and Bukry, D., 1980. Supplementary modification and introduction of code numbers to the low-latitude coccolith biostratigraphic zonation (Bukry, 1973; 1975). *Mar. Micropaleontol.,* 5:321–325.

Oppo, D.W., and Lehman, S.J., 1993. Mid-depth circulation of the subpolar North Atlantic during the last glacial maximum. *Science,* 259:1148–1152.

————, 1995. Suborbital timescale variability of North Atlantic deep water during the past 200,000 years. *Paleoceanography,* 10:901–910.

Rahmstorf, S., 1994. Rapid climate transitions in a coupled ocean-atmosphere model. *Nature,* 372:82–85.

Robinson, S., and McCave, I., 1994. Orbital forcing of bottom-current enhanced sedimentation on Feni Drift, NE Atlantic, during the mid-Pleistocene. *Paleoceanography,* 9:943–971.

Shipboard Scientific Party, 1995. Site 918. *In* Larsen, H.C., Saunders, A.D., Clift, P.D., et al., *Proc. ODP, Init. Repts.,* 152: College Station, TX (Ocean Drilling Program), 177–256.

Weaver, A.J., and Hughes, T.M.C., 1994. Rapid interglacial climate fluctuations driven by North Atlantic ocean circulation. *Nature,* 367:447–450.

Weaver, P.P.E., and Clement, B.M., 1986. Synchroneity of Pliocene planktonic foraminiferal datums in the North Atlantic. *Mar. Micropaleontol.,* 10:295–307.

Ms 162IR-105

Note: For all sites drilled, core description forms ("barrel sheets") and core photographs can be found in Section 3, beginning on page 391. Forms containing smear slide data can be found in Section 4, beginning on page 1147. On the CD-ROM enclosed in the back pocket of this volume are all tables from this chapter (including an extended coring summary table) and shipboard measurements (files containing GRAPE density, *P*-wave velocity, natural gamma radiation, magnetic susceptibility, index properties, and spectral reflectance data).